9-21-2010

Ictal Functional Neuroimaging of Childhood Absence Epilepsy

Matthew Vestal

Ictal Functional Neuroimaging of Childhood Absence Epilepsy

A Thesis Submitted to the
Yale University School of Medicine
in Partial Fulfillment of the Requirements for the
Degree of Doctor of Medicine

by
Matthew Vestal
2010

Abstract

ICTAL FUNCTIONAL NEUROIMAGING OF CHILDHOOD ABSENCE EPILEPSY
Matthew Vestal (Sponsored by Hal Blumenfeld). Departments of Neurology, Neurobiology, and Neurosurgery, Yale University School of Medicine, New Haven, CT.

Absence seizures in Childhood Absence Epilepsy (CAE) are 5 – 10 second episodes of impaired consciousness that are characterized on electroencephalography (EEG) by frontally-predominant, 3 – 4 Hz spike and wave discharges (SWD). The aims of this study were to use simultaneous EEG, functional magnetic resonance imaging (fMRI), and behavioral testing to identify the neural networks involved in absence seizures as well as to examine the timecourse of those ictal fMRI changes. It was hypothesized that absence seizures involve wide-reaching neural networks including the areas traditionally associated with normal attention processing and that absence seizures produce fMRI signal changes not only during the seizure, but before and after it as well. In this study, we recorded 88 absence seizures from a cohort of 42 children with pure CAE. These seizures were recorded as subjects participated in simultaneous EEG-fMRI scanning while engaged in a continuous performance task (CPT) of attentional vigilance or a repetitive tapping task (RTT) requiring repetitive motor activity. Using a novel, voxel-based percent fMRI change analysis combined with a volume of interest analysis, the second-by-second fMRI signal timecourse of the absence seizures were examined across numerous brain regions of interest, from 20 seconds before seizure onset through 40 seconds after seizure onset. EEG frequency analysis revealed seizures with a mean duration of 6.6 seconds and an abrupt onset and ending that were comprised of frontally-predominant, 3 – 4 Hz SWD. Ictal behavioral testing demonstrated abrupt onset of impairments during periods of SWD. These behavioral impairments were typical of CAE absence seizures in that impairments were greater in the CPT of attentional vigilance (omission error rate, OER = 81%) than in RTT testing (OER = 39 %) ($p < 0.003$). The ictal fMRI changes we observed varied depending upon the method of fMRI signal analysis used. Using the traditional general liner model, and assuming the standard hemodynamic response (HRF) function, this study replicated results consistent with previous ictal absence fMRI studies – showing ictal activations primarily in the thalamus and ictal deactivations in traditional ‘default mode’ areas. Using a more data-driven,

novel voxel-based fMRI percentage change analysis to examine the ictal fMRI timecourse on a second-by-second basis, both ictally as well as pre- and post- ictally, this study, however, demonstrated ictal involvement of diverse brain regions before, during, and after the seizure. Activation was demonstrated up to 16 seconds before seizure onset, starting first in the parietal and orbital-medial frontal cortices and progressing to lateral frontal and lateral temporal cortices followed by the occipital and Rolandic cortices and finally the thalamus. Deactivation followed a similar anatomic progression and lasted up to 17 seconds after the end of SWD. These findings reveal a complex and long-lasting sequence of fMRI changes in CAE absence seizures that are not detectable by conventional HRF modeling and are important in the understanding and eventual treatment of absence seizures associated with CAE.

Acknowledgements

I would like to thank Heather Speller for her unfailing support, unwavering friendship, and boundless love throughout my time at Yale -- both in and out of the lab. You are my everything, my love, and I don't know what I would do without you.

As a mentor, Hal has been everything that a student could hope for – both personally and professionally. As a friend and teacher, he shepherded me through the field of epilepsy and was a great influence in my choice of career. He is an amazing scientist, a first-rate mentor, and an even greater man. Hal, I can't thank you enough.

Thanks especially to my collaborators Michiro Negishi, Rachel Berman, Matt Desalvo, Clemente Vega, Marisa Spann, Todd Constable, Rusty Novotny, Brendan Killory, and Xiaoxiao Bai who were instrumental in the human side of my work. I also wish to thank those community neurologists who referred patients for this research as well as April Levin, Joshua Klein, Ulrich Schridde, and Chhitij Bashyal, without whom my previous animal work would have been impossible.

The work presented in this thesis was supported by a Howard Hughes Medical Institute Medical Student Research Training Fellowship, an American Epilepsy Society Young Investigator Award, a Yale University School of Medicine Summer Research Student Fellowship, the Yale University School of Medicine Office of Student Research, NIH R01 NS049307, and by the Betsy and Jonathan Blattmachr family.

Table of Contents

Chapter 1: Introduction to Childhood Absence Epilepsy

1A: Introduction to Epilepsy

Epilepsy is a problem with a wide-reaching influence on humanity. Affecting roughly 1 % of the world's population, epilepsy is a heterologous spectrum of disorders (1). An umbrella term used to describe a group of syndromes, epilepsy is defined as a disease state that includes recurrent spontaneous seizures arising from aberrant electrical activity within the brain. A seizure is an episode of transient abnormal electrical activity manifest clinically by changes in motor control, sensory perception, behavior, and/or autonomic function (2).

As seizures can also vary widely in the way they are clinically displayed, discussion of epilepsy is benefited from the characterization of seizures into groups. Traditionally, seizures have been first divided into focal and generalized sub-types. Focal seizures are ones that arise from neural networks confined to one cerebral hemisphere, whereas generalized seizures originate within, and rapidly engage, bilaterally distributed neural networks.

Focal (also known as partial) seizures can be further broken down into three subgroups; simple, complex, and secondarily generalized (2, 3, 4). Simple focal seizures do not include impairment of consciousness/responsiveness. These include seizures with observable motor and/or autonomic components as well as episodes normally referred to as auras -- seizures involving objective sensory or psychic phenomena. Complex focal seizures are typified by the disruption of consciousness/responsiveness. Secondarily generalized seizures begin as either simple or complex focal seizures and then evolve to bilateral convulsive seizures.

Generalized seizures can also be further classified into the following sub-groups: tonic-clonic, absence, myoclonic, and atonic seizures. Tonic-clonic seizures are typified by periods of tonic and/or clonic activity. During tonic periods, skeletal muscle contraction is prolonged, while during clonic periods, muscle contraction and relaxation quickly follow each other in rapid cycles. Myoclonic seizures are characterized by singular or irregularly recurrent clonic events, and atonic seizures are ones in which brief lapses of muscle tone are exhibited. Absence seizures (also known as petit mal seizures) are epitomized by brief periods of loss of consciousness followed by quick, deficit-free recovery from the episode.

There are several common clinical syndromes that include absence seizures – namely Childhood Absence Epilepsy, Juvenile Absence Epilepsy, and, to a lesser extent, Juvenile Myoclonic Epilepsy. Of these, Childhood Absence Epilepsy is the most common. It is the subject of much of the following thesis and will therefore be described in further depth.

1B: Childhood Absence Epilepsy

Childhood Absence Epilepsy (also known as pyknolepsy) is a relatively common sub-type of idiopathic generalized epilepsy. Childhood Absence Epilepsy (CAE) affects approximately 10% of all children with epileptic disorders and is characterized by seizures lasting 3 – 10 seconds. Typical absence seizures consist of brief episodes of staring and unresponsiveness that are, intermittently, accompanied by subtle myoclonic jerks or eyelid fluttering (5). In severe forms of untreated disease, up to hundreds of seizures can occur per day, without any obvious deficits present after the conclusion each seizure (6).

Onset of absence seizures is typically between the ages of 5 and 7 years, and most children outgrow the seizures in adolescence. In practice, seizure control can be obtained in roughly 60 - 80% of CAE cases through the use of medications such as ethosuximide, sodium valproate, or lamotrigine (7). CAE seizure triggers are similar to triggers in other forms of epilepsy, with seizures more likely to arise after hyperventilation, photic stimulation, sleep deprivation, or medication withdrawal.

Though seizure control is often possible though medication, CAE is by no means a benign diagnosis (8). In up to 40% of cases, children with CAE can develop generalized tonic-clonic or grand mal seizures (9). Children with CAE also have particular problems in academic settings, even between their seizures. They are more likely than their peers to have below average academic performances, repeat a grade, and drop out of high school. Children with CAE also have higher rates of teenage pregnancy and alcohol-related problems. CAE predisposes children to go on to be more likely to hold unskilled jobs and report poor job satisfaction (10).

As such, it is of utmost importance to diagnose CAE as early as possible so that children with the disease can receive the help that they need in order to address their particular psycho-social and academic difficulties. Frequently however, the disease is mistaken as inattentiveness or daydreaming in school settings, and children go long periods before they are brought to clinical attention.

In order to be diagnosed with CAE, children must exhibit both the phenotypic absence seizures described above as well as the characteristic electroencephalographic findings associated with CAE. Electroencephalography (EEG) in patients with CAE reveals large amplitude, bilateral, frontally predominant, 3-4 Hz discharges that have a

characteristic spike and wave pattern (Fig. 1). This 3-4 Hz electrographic pattern, called spike and wave discharges (SWD), is pathognomonic of CAE.

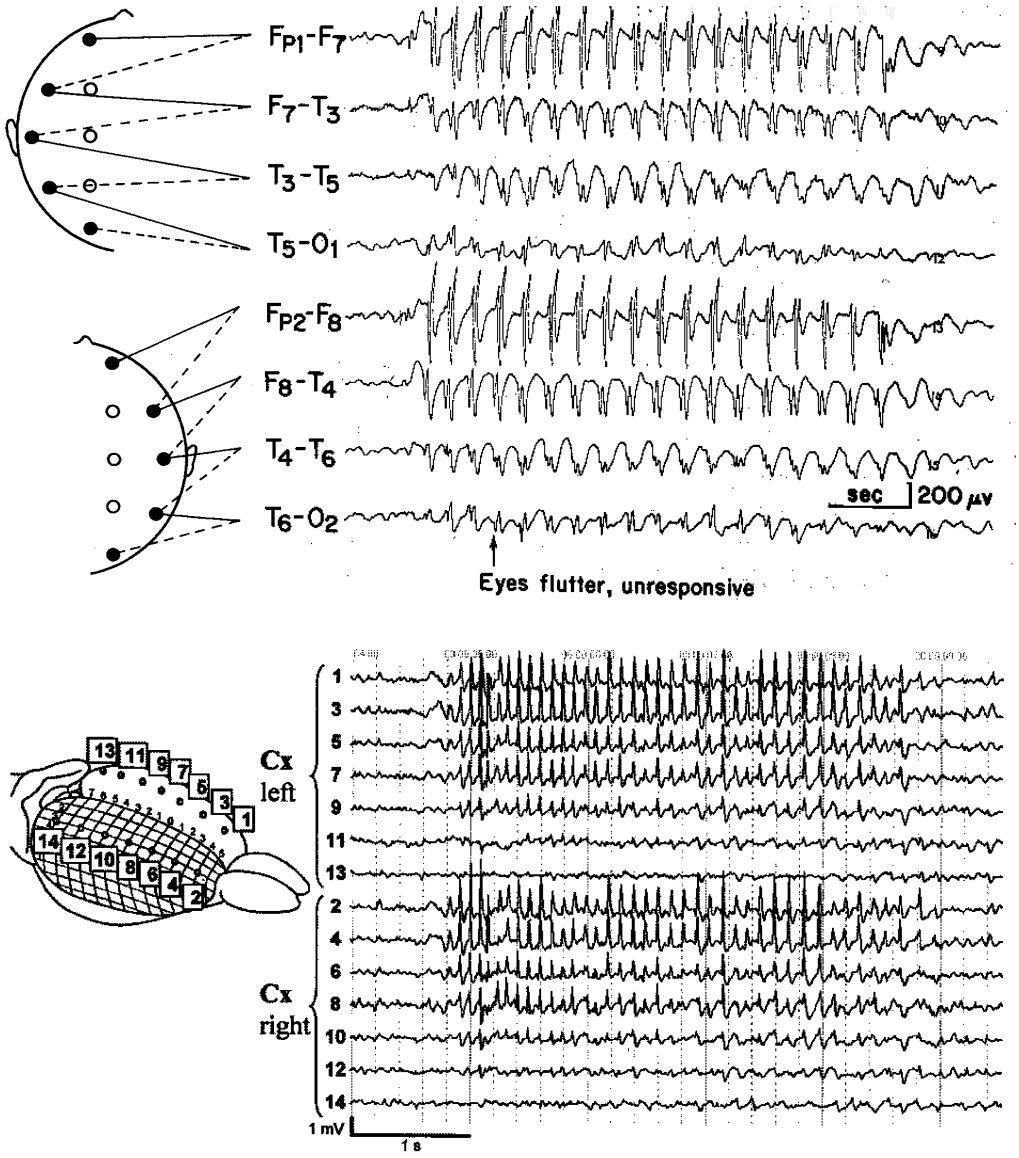

Figure 1. Typical spike-wave EEG discharges during absence seizures have a focal frontal predominance. (Top Panel) EEG recording from a 7-year-old girl during a typical absence seizure reveals bilateral, synchronous 3–4 Hz spike-wave discharges, with an anterior to posterior amplitude gradient. (Inset of electrode positions modified with permission from Fisch, B.J. (1991) Spehlmann's EEG Primer. Elsevier, Amsterdam. EEG recording modified with) (Bottom Panel) Electrocorticography from the surface of the WAG/Rij rat (an animal model of CAE) cortex during spike-and wave seizures reveals intense involvement of the anterior cortex and relative sparing of the occipital lobes. (Reprinted with permission from Vestal, et al, 2010. Copyright 2010, Springer.)

1C: Spike and Wave Discharge Pathophysiology

The generation of the hallmark SWD of CAE lies in the rhythm generating function of the basic thalamocortical circuit detailed in Fig. 2. In this physiologically normal circuit, projections from the thalamus synapse on pyramidal cells and interneurons in the cerebral cortex as well as on inhibitory neurons in the nucleus reticularis (NRT). Layer VI of the cortex reciprocally innervates the same area of the thalamus from which the afferent thalamic projection is received, and the NRT returns inhibitory projections to the thalamus. Cerebral cortex, NRT ***and*** the thalamus must all be present within the circuit in order to generate the typical 3-4 Hz SWD that underlie absence epilepsy (5).

Low threshold (T-type) calcium channels are ubiquitous in thalamic neurons and influence thalamic oscillatory behavior in both physiologic (i.e. sleep-spindles) and pathophysiologic (i.e. SWD) states. These T-type calcium channels only recover from inactivation to become available for reactivation at relatively hyperpolarized resting membrane potentials (between -70 and -80 mV). As such, another intrinsic thalamic current, the hyperpolarization activated cationic current, I_h, is required in order to generate oscillatory activity. Carried by both Na^+ and K^+ ions, the I_h current is activated by hyperpolarization to potentials less than -60mV. The I_h current activates slowly and results in the generation of a depolarizing pacemaking potential (Fig.3). Inhibition of thalamic neurons activates this I_h current, and activation of the I_h current leads to depolarization, which in turn triggers T-Type calcium channels. This physiologic activity creates the oscillating pattern of 10-15 Hz sleep spindles characteristic of normal sleep.

This activity, however, with just small changes in the circuit, can also create abnormal oscillations such as SWD (11).

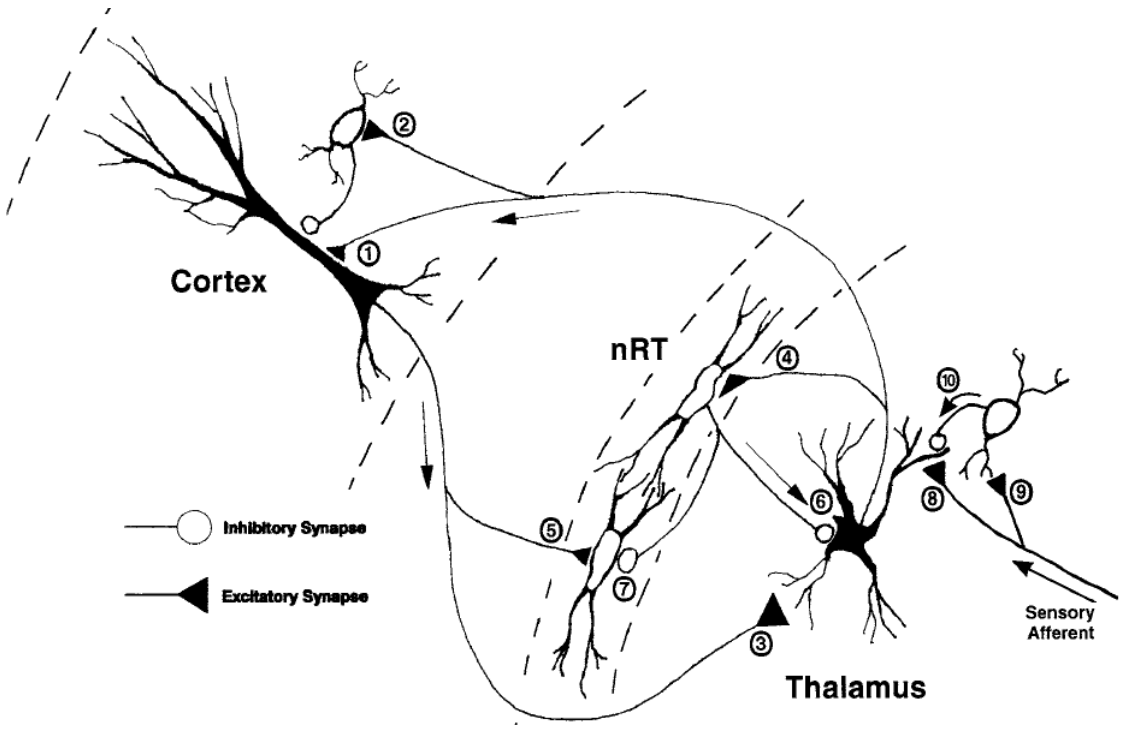

Figure 2. The basic thalamocortical circuit. Thalamic neurons in primary sensory relay nuclei project to layers III and IV and V and VI of the cerebral cortex. These projections terminate on both the pyramidal neurons (synapse 1) and on inhibitory interneurons (synapse 2) in the cortex. Layer VI pyramidal neurons reciprocally innervate the same area of the thalamus from which an ascending afferent is received (synapse 3). Both the thalamocortical and the corticothalamic projections send an axon collateral to nucleus reticularis thalami (nRT; synapses 4 and 5). Nucleus reticularis thalami provides inhibitory GABAergic innervation to the thalamus (synapse 6) and to other NRT neurons (synapse 7). The major sensory afferents to the thalamus synapse onto the dendrites of both thalamic relay neurons (synapse 8) and inhibitory interneurons (synapse 9). The dendrites of inhibitory interneurons can function as both pre- and postsynaptic elements and can provide inhibitory innervation of thalamic relay neuron dendrites (synapse 10), as well as conventional axonal synaptic connections (synapse 10). (Reprinted with permission from Blumenfeld and Coulter, 2008.)

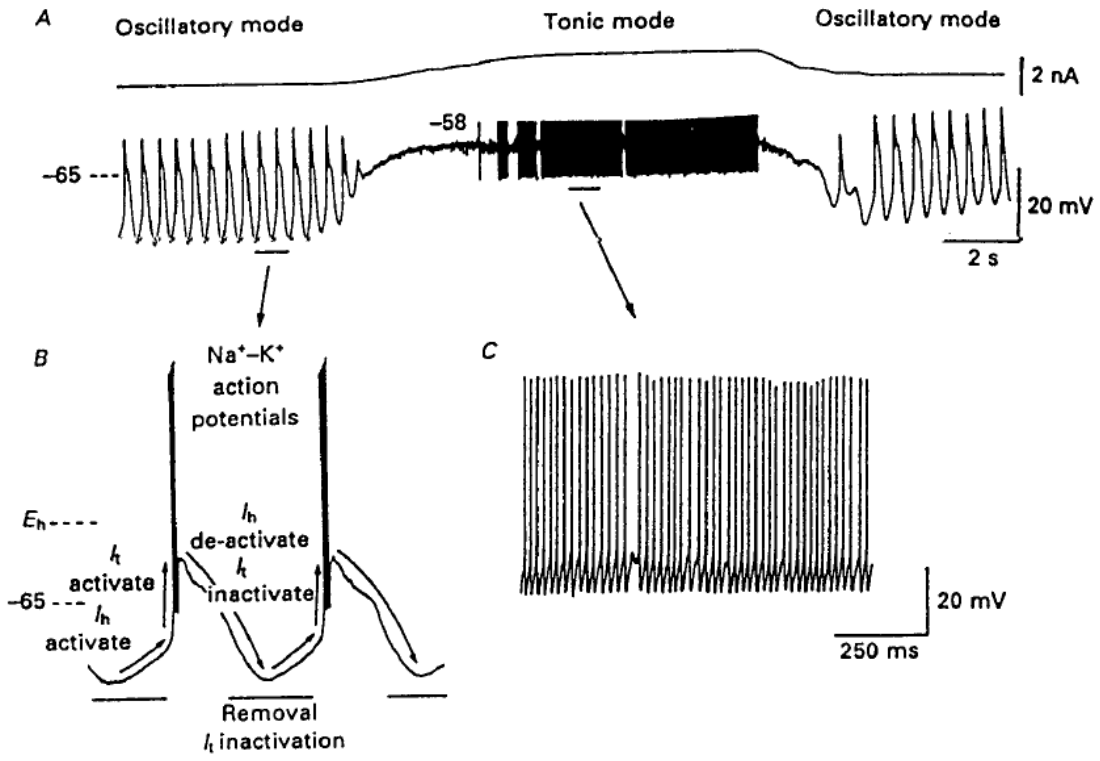

Figure 3. Oscillatory and tonic firing modes of thalamic neurons. **A, B**: The interaction of T current (I_t) and I_h results in the generation of spontaneous oscillations in thalamic neurons. **A, C**: Depolarization of thalamic neurons inactivates I_t, causing transition from oscillatory firing mode to tonic relay mode. (Reprinted with permission from McCormick DA et al. Properties of a hyperpolarization-activated cation current and its role in rhythmic oscillation in thalamic relay neurons, J Physiol. 1990; 431:291-318.)

In absence epilepsy, pathologically enhanced excitability leads to the massive abnormally synchronous oscillations underlying SWD. This enhanced cortical excitability in CAE leads to increased cortical firing rates. Increased rates of cortical firing, through corticothalamic projections (Fig. 4a), produce sustained NRT activity – changing the inhibition experienced by the thalamus. Normally, non-pathologic firing rates of the NRT lead to thalamic inhibitory postsynaptic potentials (IPSPs) of 100 msec (mediated by $GABA_A$ receptors). These normally fast IPSPs lead to a thalamic

oscillation frequency typical of sleep spindles (10-15 Hz). However, with sustained NRT firing and concomitant activation of $GABA_B$ receptors, thalamic IPSPs grow to 300 msecs (12). It is these 300 msec thalamic IPSPs that set the oscillation frequency of the thalamus to a slower 3-4 Hz, creating the SWD typical of absence epilepsy (Fig. 4b) (5).

1D: Simultaneous Electroencephalography, Functional Magnetic Resonance Imaging, and Behavioral Testing in Childhood Absence Epilepsy

In the past decade, functional magnetic resonance imaging (fMRI) with simultaneous EEG has been used to study seizures with characteristic SWD – including absence seizures (6, 13-17). These methods have revealed blood oxygenation level-dependent (BOLD) changes in cortical and subcortical areas during the electrographic course of spike-and-wave seizures. Other studies, in both humans (18 – 29) and animals (30 – 32) have suggested that these BOLD fMRI changes during SWD are likely a reflection of underlying changes in neuronal activity during these seizures. Consistently, studies using concomitant EEG and fMRI have demonstrated fMRI BOLD signal increases in bilateral thalamus and decreases in medial and lateral parietal cortices during spike-and-wave seizures – suggesting the likely involvement of these areas in the disease process. These studies, however, have not been able to correlate these fMRI changes with impaired ictal behavior, however, and, thus, it is impossible to determine whether the fMRI BOLD signal changes reported are those that are co-occurring with the ictal impairments that so dramatically affect the lives of patients with childhood absence epilepsy.

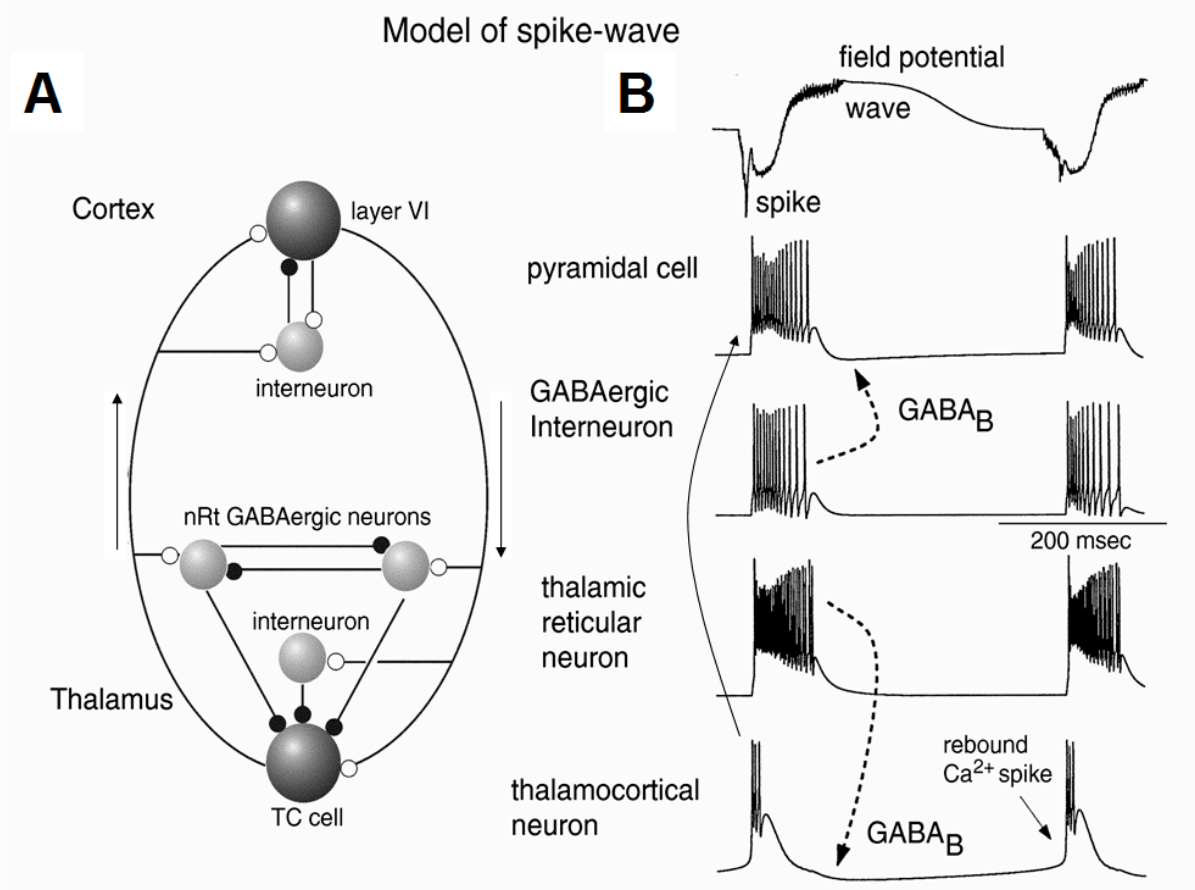

Figure 4. Cortical and thalamic cellular networks involved in spike-and-wave seizure generation. **A**: Simplified circuit diagram of cortical and thalamic networks shown in Figure 2, involved in both normal spindle wave oscillations and spike-and-wave oscillations. Cortical pyramidal neurons and thalamocortical cells form reciprocal excitatory connections (*open circles*). Inhibitory GABAergic interneurons distributed throughout the cortex and thalamus, as well as in the thalamic reticular nucleus, modulate the excitatory activity (*inhibitory synaptic connections are denoted with filled circles*). **B**: Simulation of one cycle of SWD in corticothalamic networks. A burst of spikes in a thalamocortical neuron activates the cortical pyramidal cell through excitatory connections. This generates a strong burst of action potentials through intracortical recurrent excitatory connections. This burst strongly activates both local GABAergc neurons and thalamic reticular neurons. Activation of $GABA_B$ receptors produces a slow IPSP, leading to a rebound Ca^{2+} spike in the thalamocortical cell 300 msec later, and initiating the next cycle of the oscillation. (Reprinted with permission from McCormick DA et al. Properties of a hyperpolarization-activated cation current and its role in rhythmic oscillation in thalamic relay neurons, *J Physiol*. 1990; 431:291-318.)

In the past, behavioral testing alone (i.e. without functional neuroimaging) during absence seizures has been used to examine ictal impairment in CAE. Using behavioral testing and simultaneous EEG during childhood absence seizures, a tight temporal correlation between scalp EEG detection of SWD and behavioral impairment during seizures has been demonstrated. This work has shown that tasks requiring decision making, attention, and/or verbal responses are most severely affected during absence seizures while repetitive tasks or simple reaction time tasks are often spared (6, 14).

While work in the field has demonstrated the fMRI changes during electrographic absence seizures and, separately, the types of behavioral impairment typical of childhood absence epilepsy, no studies to date have used simultaneous EEG-fMRI *and* behavioral testing to examine how BOLD signal changes during absence seizures vary with ictal behavioral impairment. Moreover, all previous studies have looked at fMRI signal changes only during the presence of SWD. Recent studies have shown that BOLD signal changes in neural networks associated with CAE can both begin before and long outlast electrographic absence seizures (48, 54, 55). It is the goal of this thesis to fully examine BOLD signal changes during ictal behavioral testing as well as the timecourse of those ictal BOLD signal changes through the following specific aims.

1E: Specific Aims and Thesis Outline

The aim of this thesis is to explore the fMRI signal changes associated with absence seizures in childhood absence epilepsy. Specifically, the objectives for this thesis are:

1) Using simultaneous EEG, fMRI and behavioral testing, examine ictal fMRI signal changes during behavioral testing in childhood absence epilepsy

2) Examine the time course of fMRI signal change in childhood absence epilepsy, not only during the presence of SWD on EEG, but particularly before and after the electrographic ictal period.

In sections 2A, 3A, and 4A, this thesis explores Specific Aim 1, using simultaneous EEG and fMRI to demonstrate the ictal involvement of specific neural networks during behavioral impairment on two separate behavioral tests.

In sections 2B, 3B, and 4B, this thesis answers Specific Aim 2. In these sections, this thesis examines the timecourse of fMRI signal change in typical childhood absence seizures – focusing on fMRI changes not only during the period of SWD, but BOLD signal changes both before and after this period. These sections also compare the timecourse of BOLD signal change in different regions of interest in the brain, examining the similarity of ictal fMRI signal percentage change across these regions of interest

Chapter 4, discusses the meaning and implications of as well as the conclusions drawn from the results reported in chapter 3 and explores several interesting future directions of this work.

Chapter 2: Methods

2A: Ictal Imaging Methods: Simultaneous EEG-fMRI and Behavioral Testing during CAE

Patients with childhood absence epilepsy have profound ictal behavioral impairments. Previous work using EEG recording during behavioral testing has shown that, during absence seizures, children have more difficulty with tests of attentional vigilance than they do with tests requiring simple repetitive motor performance (14).

Prior ictal fMRI recording of children during absence seizures, but without behavioral testing, has shown consistent BOLD signal increases in bilateral thalamic areas and BOLD signal decreases in medial and lateral parietal cortices (18 – 28). Using tests of attentional vigilance and repetitive motor performance, this section (section 2A) describes the methods used in the elucidation of the pattern of ictal fMRI signal change in children with pure CAE who are actively engaged in a behavioral task. To our knowledge, this is the first experiment that uses simultaneous EEG-fMRI and behavioral testing in order to better examine the areas of ictal BOLD signal change during seizures with documented behavioral impairment.

I: Subjects

All procedures involving human subjects were approved by the human investigation committee, the institutional review board at Yale University School of Medicine, and by the Yale Magnetic Resonance Imaging Center.

Thirty-seven children between 6 and 18 years of age who were diagnosed with typical childhood absence epilepsy were referred by their pediatric neurologists and participated in this study after written informed consent. Subjects were permitted to participate in the study providing they met the following inclusion criteria:

1. Age: 6 – 18 years
2. Clinical diagnosis of childhood absence epilepsy based on International League Against Epilepsy criteria (3) with diagnosis confirmed through a strict neurological history performed by trained staff
3. EEG with typical 3-4 Hz bilateral, frontally predominant SWD and normal background activity; EEGs were reviewed for these characteristics by an outside neurologist as well as well as by a neurologist affiliated with the study in all cases (HB)

Exclusion criteria were:

1. Known organic or structural brain abnormality
2. Additional seizure phenotypes (such as myoclonic, tonic-clonic, or partial seizures)
3. Other neurological disorder

II: Subject Training

Prior to participation in simultaneous EEG-fMRI scanning and behavioral testing described below, subjects underwent a training session on a separate visit approximately two weeks before participating in the actual scan. This training session familiarized subjects with the scanner environment, the sounds of the fMRI scanner, the layout of the

scanning environment, the research personnel, and the behavioral tasks. During training, subjects practiced each behavioral task in a mock fMRI scanner while they were rated on their ability to minimize movement while in the mock scanner. After this session, feedback regarding ability to minimize movement was given to parents along with a compact disc (CD) recording of the fMRI sounds. Parents were encouraged to have the subjects practice lying still while the fMRI sounds played and parents observed the subjects movement. Parents were then asked to provide subjects with feedback, practicing with the CD in order to minimize any unnecessary movement during the eventual scanning periods.

III: Medication withdrawal

It has been demonstrated that, in the CAE population, the incidence of absence seizures is modulated by vigilance and attentional state, with seizure frequency trending downward as children are more attentionally vigilant. As, in this experiment subjects are engaged in a task of attentional vigilance while being scanned, it was necessary to develop a method for increasing the frequency of seizures during the experimental paradigm in order to sufficiently power the examination of behavioral performance and fMRI activation changes during the absence seizures.

Previous studies have used seizure triggers such as hyperventilation, sleep deprivation, and/or photic stimulation as known methods for increasing seizure frequency. However, this study did not use these techniques as they had the potential to complicate the interpretation of attentional data or fMRI BOLD signal change. Alternatively, in selected subjects, we used medication withdrawal as our only method to increase the probability of recording an absence seizure during simultaneous EEG-fMRI

and behavioral testing (33 – 36). Specifically, all subjects who were on medication prior to the study, were asked to abstain from taking their medication for up to 48 hours before the EEG-fMRI recording.

In all 37 subjects, who participated in the study, none had any sustained worsening of their absence seizures, emergence of other seizure types, or other adverse effects from medication withdrawal. Subjects and parents were advised that, during periods of medication withdrawal, subjects should not ride bicycles, swim, or operate any heavy or dangerous machinery. Participation in the study and medication withdrawal was discussed with the subjects' primary neurologist and a trained neurologist was on call and available to participants for the duration of medication withdrawal in the case of any questions or adverse events. While off medication, it was ensured that subjects would be under the constant supervision of a parent or other responsible adult and subjects were contacted at least once per day to monitor their well-being while off medications. Medication withdrawal typically occurred during a weekend or holiday period to minimize the effect of increased seizures on subjects' school performance and medications were immediately re-started after the conclusion of the EEG-fMRI recording period.

Prior to participation in fMRI scanning, participants and family members were queried as to the frequency and duration of the subjects' absence seizures at time of diagnosis as well as both during and directly before medication withdrawal.

As the mean half life of ethosuximide is approximately 30 hours, 11 hours for valproic acid, and 32 hours for lamotrigine, it is possible that the subjects full bodily medication load had not been excreted by the time of EEG-fMRI recording. Even if the

subject still had a small amount of circulating medication, the amount of drug on board at the time of the fMRI scanning was not thought to influence performance on the behavioral tasks or fMRI activity pattern or deleteriously decrease seizure frequency. The 48 hour withdrawal period was chosen to balance efforts to increase seizure frequency during scanning with efforts to maintain participant safety.

IV: EEG recording and Analysis:

EEG recordings in subjects 1-7 (see subject numbering in Section 2C, Part I) were performed with an EEG cap with silver/silver-chloride electrodes (modified from Quik-Cap 21 channel, Neuroscan Inc., North Carolina, U.S.A.), carbon fiber cables (in-house), a 125Hz analog low-pass Butterworth filter (in-house), and an EEG recorder (NuAmps, Neuroscan Inc.). In these subjects, EEG signal was digitized at 500Hz with 32-bit DC recording and displaying output using a standard 10-20 lead montage. EEG in subjects 8-9 was recorded similarly, except that carbon wire EEG electrodes were used (in-house), 32 channels were obtained, a pre-amplifier was introduced (in-house) (37), and the signal was digitized at 1000Hz with a newer EEG recorder (SynAmps2, Neuroscan Inc.). All EEG signals were recorded with respect to a ground electrode (located anterior to Fz) and re-referenced at the time of EEG visual review to Cz reference, linked ears reference, and to a sagittal bipolar montage. A combination of SCAN (Neuroscan) software and in-house temporal principal component analysis (PCA) software were used for filtering magnetic resonance artifact (38) to create an EEG image where SWD could be identified on visual inspection (Fig. 5). Adaptive noise cancellation software was used for filtering in subject 8 (37).

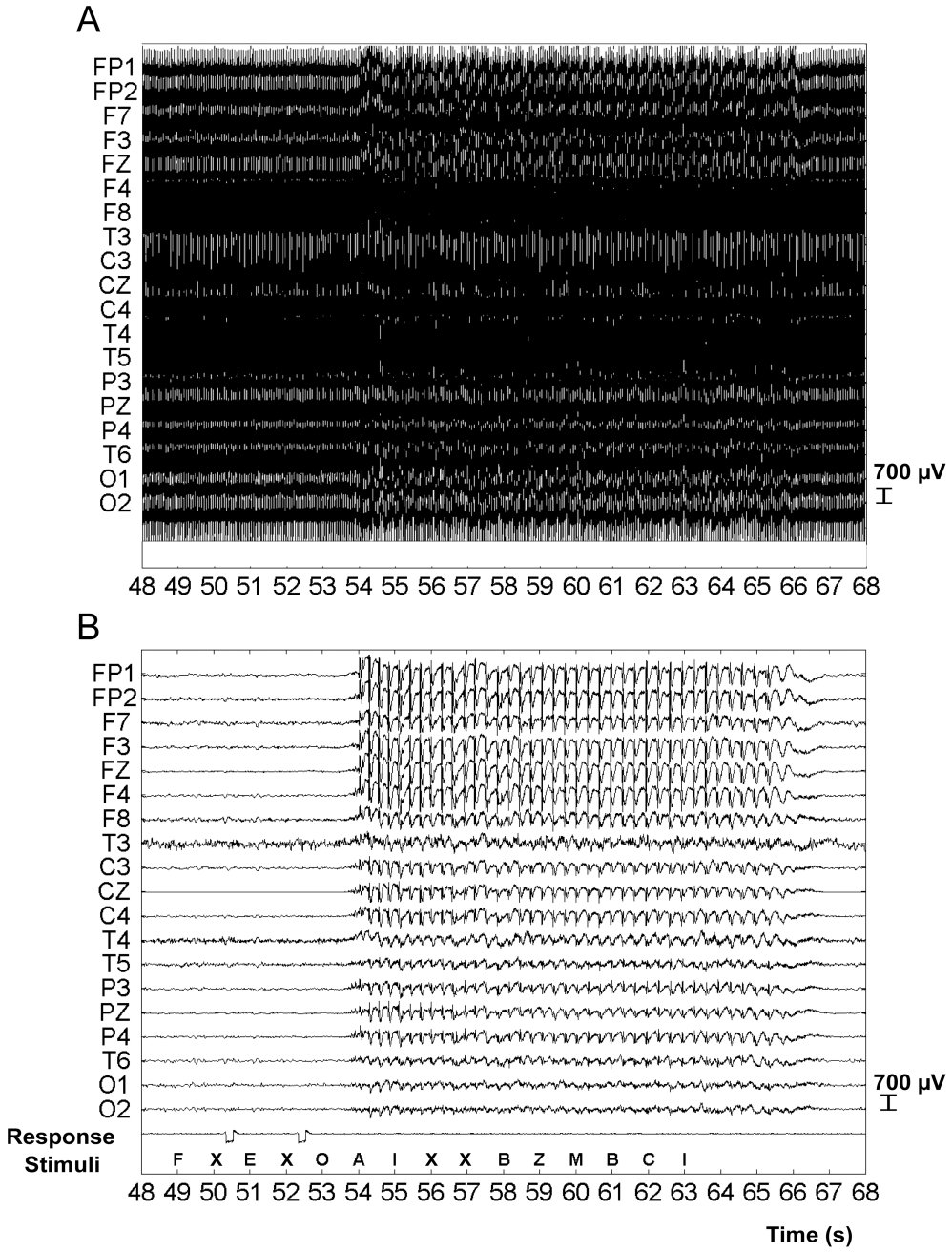

Figure 5. Simultaneous EEG, fMRI and behavioral testing with artifact removal. Linked-ears referential EEG recording of a 12 second absence seizure in Subject 1. A) EEG prior to adaptive PCA-based artifact removal and B) EEG from the same seizure after artifact removal. The recording shows a typical large amplitude bilateral 3 Hz spike-wave discharge. The patient responded to target X during CPT testing prior to seizure onset (voltage deflections on EEG channel labeled "Response"). However, when the targets occurred during the seizure, the patient was unable to respond.

After each EEG was recorded it was low-pass filtered at 25 Hz and visually inspected for SWD showing a frequency of 3-4 Hz. This visual inspection was done by a team of at least three trained research personnel, one of whom (HB) was a neurologist with significant experience in identifying typical 3 – 4 Hz SWDs. During visual inspection, SWD onset and end times were determined to within a 0.1 second time resolution and these times were then used for all subsequent EEG, behavioral, and fMRI analyses.

An example of an EEG prior to, and following, artifact removal is shown in Fig 5. After signal processing as described above, the in-magnet EEG shows sufficient quality to clearly reveal SWD (Fig 5b).

Prior to simultaneous EEG-FMRI recording, approximately five minutes of out-of-magnet EEG data were collected in a room adjacent to the scanner in order to test the proper output of the recording device, record EEG with any non-scanner related noise (i.e. cardiac), and to potentially obtain out-of fMRI EEG recordings of typical seizures. Once the subject was inside the MRI scanner, continuous EEG recording occurred until the subject was removed from the scanner. Two minute intervals of no-fMRI-scanning EEG collection were included between successive runs of fMRI data acquisition in order to collect artifact-free (gradient and radio frequency), in-magnet EEG data. The out-of-magnet EEG data and EEG data between fMRI scans were used for PCA-based ballistocardiogram and scanner noise removal from the in-fMRI EEG data, respectively (38).

To ensure correct synchronization of EEG, fMRI and behavioral testing data, the initiation of the stimulus presentation program (described below in Section 2B, Part VI)

was triggered by a transistor-transistor logic (TTL) pulse from the MRI scanner. In addition, the behavioral stimulus presentations and button push responses were recorded by the presentation software as well as in separate channels by the EEG recorder.

V: fMRI Data Acquisition and Analysis

Subjects were instructed to lie on their backs with their heads secured in the head coil using a Velcro strip. Subjects' arms were placed at their sides and supported by foam padding. Ear plugs were placed inside subjects' ears and subjects' were fitted with a headset and microphone so that they could communicate with fMRI operators in case of emergency. Additional foam padding was placed around the headset to further secure the head and minimize movement within the scanner. Subjects were asked to hold a button box in their right hand and were asked to use their right thumb to press the button whenever necessary according to the below behavioral testing paradigm.

Imaging was performed on a 3 Tesla Magnetom Trio scanner (Siemens Medical Systems, Erlangen, Germany). Prior to behavioral testing, anterior commissure-posterior commissure (AC-PC) aligned axial, T1 anatomical images were acquired in the same image plane as the fMRI data that would follow. These anatomical images were T1 spin echo images with a repetition time of 300 msec, echo time of 2.47 msec, matrix size of 256 x 256, slice thickness of 6 mm, 25 slices per image, and a field of view of 22 cm. After T1 anatomical images were acquired, functional MRI images were acquired during simultaneous EEG recording and behavioral testing using an echo planar imaging (EPI) BOLD sequence with a repetition time of 1550 msec, an echo time of 30 msec, a flip angle of 80, and a matrix size of 64 x 64 with all other parameters the same as the T1

anatomical acquisition series. Each fMRI scanning period lasted for 10 minutes and 40 seconds. Up to 6 (typically 3 or 4) fMRI scanning periods were obtained per recording day, as tolerated by subjects.

fMRI data were analyzed using SPM2 software (http://www.fil.ion.ucl.ac.uk/SPM) on a Matlab 6.5 platform (MathWorks, Natick, MA). Images were first realigned to the initial scan of each 10 minute and 40 second functional scanning series. Images were then spatially normalized to the SPM EPI template (in Montreal Neurological Institute or MNI Space). Images were spatially smoothed using a 10 mm full width at half maximum Gaussian kernel. In each 10 minute and 40 second fMRI scanning period, the initial 10 image acquisitions (the first 15.5 seconds) were discarded in order to control for initial variations in the scanner's magnetic field. All results for functional data are displayed superimposed on the Montreal Neurological Institute brain template "colin27" (single_subj_T1 in SPM) in radiological convention.

Timing of BOLD signal change was determined in relation to EEG SWD by acquisition of TTL image synchronization signals acquired with EEG recording. fMRI changes during seizures were modeled using a standard double gamma hemodynamic response function, HRF. The parameters for the hemodynamic response function used for the model are documented in the SPM_HRF.m file with a delay of response relative to onset of 6 sec, a delay of undershoot relative to onset of 16 sec, dispersion of response and dispersion of undershoot of 1, a ratio of response to undershoot of 6, an onset at 0 sec and a kernel length of 32 sec. This resulted in the use of the typical SPM HRF with a peak time of 5.1 sec and an undershoot nadir time of 15.8 sec.

Seizure onset and duration were determined from the EEG and were used to define a box-car function which was convolved with the HRF. The 32 second per block design of the behavioral testing described below was also included in the model in order to remove BOLD signal changes due to the behavioral paradigm.

A t-test was used to identify BOLD signal changes during seizures that were significantly different than signal changes during periods without seizure. In doing this, a single subject analysis was used, combining seizures within each subject. Extent threshold, k, was set at 3 voxels. To correct for multiple comparisons, we used the false discovery rate (FDR), with an FDR-corrected p-threshold of 0.05 (23, 26, 39 – 40). Data using this FDR correction method produced the same general results as our analysis with an uncorrected voxel-level height threshold of $p = 0.001$ (data not shown).

In order to correct for any movement made by the subject, realignment plots showing 3 axes of both translational and rotational motion were examined for every fMRI scanning period. In all cases, transient movement during seizures was less than 1 degree in rotation and less than 3mm in translation, with one exception (one scanning period for subject 8, that was therefore excluded). There were, however, transient subject movements that were greater than 3mm in translation and 1 degree in rotation that occurred when subjects were not seizing. In order to account for this, we repeated the above-described, single-subject SPM analysis, accounting for the 3 possible rotational (pitch, yaw, and roll) and 3 possible translational (x, y, and z) movement parameters. This analysis is included in Fig. 8 for comparison to the non-motion-corrected results shown in Fig. 7.

VI: Behavioral Tasks and Analysis

To test subject's ictal behavior, we used two simple, button-press tasks that have been used previously by pioneers in the field of ictal CAE behavioral testing (14, 42, 43).

a) Projection Set-up

All behavioral tasks were programmed using E-Prime 1.1 (Psychology Software Tools, Inc. Pittsburgh, PA). To begin each task, subjects were directed to look through mirror attached to the head coil in order to see a + in the center of the display screen. Images were projected onto a display screen in the scanner room and subjects viewed letters in their normal orientation. Button pushes were recorded via a hand-held button box in the scanner. Each subject was instructed to hold the button box in their right hand and press the button with their right thumb whenever indicated by the behavioral task instructions. To ensure correct synchronization of the data from the behavioral task, fMRI and EEG recordings, stimuli and response timing were recorded both using the E-Prime program, as well as directly on the EEG tracing (Fig 5b).

b) Continuous Performance Task

The first of the two button-press, behavioral tasks used was the Continuous Performance Task (CPT). CPT is a task that involves attentional vigilance (14). During CPT, each subject viewed a series of random letters and was instructed to push a button each time an X was displayed. When the task began, one letter was randomly selected from the 16 letter sequence A B C D E F H I L M N O T X Y Z and was projected onto the display screen. Each letter was presented, one letter at a time, at a frequency of 1 Hz and in the original position of the + sign. 25% of all letters presented were the target X,

and, thus, an X appeared once every 4 seconds on average. Each letter was displayed for 250 msec, and followed by 750 msec of a blank screen. The interval between consecutive letter onsets was 1000 msec. 32 second epochs of Fixation (see below) and CPT were alternated 10 times each in a block design, for a total behavioral task time of 10 minutes and 40 seconds per CPT scanning period.

c) Repetitive Tapping Task

The second button-press, behavioral task was the Repetitive Tapping Task (RTT) – a task that requires repetitive motor system performance and minimizes attentional vigilance (14). The RTT was identical to the CPT except that subjects were instructed to push the button for *every* letter they saw and that no X's were included in the letter sequence presented. Like with CPT, there were alternating 32 second epochs of Fixation (see below) and random letter presentations from the above letter sequence at 1 letter per second. As in CPT, multiple 10 minute and 40 second RTT scanning periods were repeated up to 4 times during scanning day. If a subject underwent multiple scanning periods within one day, the scanning periods were presented so that CPT scanning periods alternated with RTT scanning periods.

d) Fixation

Fixation refers to periods where subjects view a + sign during part of the scanning period. Fixation was used in two instances in this study. First, 32 second episodes of fixation were interleaved between 32 second periods of either CPT or RTT to create a 10 minute and 40 second CPT or RTT scanning period. Additionally, some subjects, performed 10 min 40 sec runs of "Fixation Only" scanning, during which they only

viewed a + for the entire period of fMRI imaging. For the duration of the Fixation Only scanning periods no letters were presented. Fixation Only scanning sessions were performed as internal controls to determine ictal fMRI BOLD signal change when the subject was not engaged in the CPT nor RTT task. On average, subjects performed 4 CPT/RTT/Fixation Only scanning periods per scanning day (no more than 4 of any one type, and no more than 6 total scanning periods per scanning day).

e) Behavioral Task Analysis

CPT and RTT data were analyzed for errors of omission (targets without a button press). Target for the CPT task was the letter X, and target for RTT was any letter. The interval for correct CPT responses were 120 to 1000 msec after stimulus presentation and 0 to 1000 msec for RTT. In all cases included in this study, none of the subjects responded to the target later than 1000 msec after targets during seizures.

VII: Author's Involvement

All of the above experimental sections were conducted with the express involvement of the author of this thesis including: subject recruitment, subject training, subject communication, EEG recording and analysis, fMRI acquisition and analysis, and behavioral task administration and analysis. Michiro Negishi and Rachel Berman assisted with EEG and fMRI data acquisition, and Xiaoxiao Bai and Hal Blumenfeld with fMRI analysis.

2B: Ictal Timecourse Methods : Timecourse of fMRI and behavioral changes during typical childhood absence seizures

Ictal fMRI has been increasingly used to observe BOLD signal changes in CAE. Several studies have consistently found ictal BOLD signal increases in bilateral thalamus as well as ictal decreases in medial and lateral parietal cortex in populations with SWD. Ictal BOLD signal findings in other cortical and subcortical areas, however, have thus far been inconsistent (18 – 28).

To our knowledge no studies have examined the timecourse of ictal fMRI signal change in absence seizures. In other words, there has been no examination of the change in ictal BOLD signal over time in subjects with CAE.

Additionally, it has been shown that BOLD signal changes, associated with single events, can vary from one region of the brain to another (28, 44 – 48). No studies have examined the differences in ictal BOLD signal timecourse between brain regions. As such, it is the goal of section 2B and 3B of this thesis to examine not only the overarching ictal timecourse of fMRI changes in CAE during SWD, but also to examine the differences in ictal BOLD signal timecourse that might exist between different regions of the brain.

I: Subjects

The same cohort of 37 subjects was used as is described in Section 2A. An additional 5 subjects participated in Section 2B bringing the total of participants to 42. All subjects met the inclusion and exclusion criteria described in Section 2A and participated in the below procedures with the approval of the institutional review boards at the Yale School of Medicine and the Yale Magnetic Resonance Imaging Center.

II: Subject Training

Subject training was conducted as described in Section 2A, Part II.

III: Medication Withdrawal

All subjects' medication was withdrawn as described in Section 2A, Part III.

IV: Behavioral Tasks and Analysis

All behavioral tasks (including CPT, RTT, and Fixation Only) were conducted as described in Section 2A, Part VI. Performance in CPT and RTT, however, was analyzed differently. Performance was analyzed by calculating the 'Correct Response Percentage Rate.' Correct Response Percentage Rate was calculated as (Q1/Q0) x 100, where Q0 was the number of target letters and Q1 was the number of correct responses to targets. Correct Response Percentage Rate was calculated for each subject in each task for each scanning period, using two second bins across all scanning periods. Mean CPT and RTT performance rates for each time bin were then calculated by averaging across subjects.

V: EEG Recording and Analysis

All EEG recording and visual inspection was conducted as described in Section 2A, Part IV. All EEG recordings of the 5 additional subjects included section 2B were recoded using 32 carbon wire EEG electrodes (in-house) and an in-house preamplifier (37), and the signals were digitized at 1000 Hz with the newer EEG recorder with 24 bit data resolution (SymAmps2, Neuroscan).

Here (section 2B), EEG analysis is conducted differently. For this arm of the experiment, a time-frequency analysis (49) was performed to investigate the frequency dynamics before, during, and after the SWD. Analysis was performed on EEG data from 20 seconds before through 40 seconds after the onset of each SWD. To calculate time-frequency dynamics, we used a short-time Fourier transform in MATLAB 7.1 (Mathworks, Natick, MA). This short-time Fourier transform includes a sliding time window (window width = 5.12 sec, shifted at 20 msec intervals) in order to examine the frequency composition of short sequential segments of EEG data over time. This short-time Fourier transform was conducted over a frequency bandwidth from 0 – 25 Hz, in each channel, for each subject exhibiting SWD. Low frequency <1 Hz EEG signal was observed at all times, independent of the presence of SWD, and was therefore removed during analysis using a high-pass filter (>1 Hz).

The ictal, pre-ictal (time period 20 seconds before seizure onset), and post-ictal (time period 40 seconds after seizure onset) periods were temporally aligned across each period of SWD. The ictal period of each seizure was scaled to the mean seizure duration across all subjects (6.6 sec). Pre- and post-ictal times were not scaled to either individual or mean seizure duration, they were simply aligned in time across seizures by lining up seizure onset times for pre-ictal data and then by lining up the seizure end times for post-ictal data.

Power spectra for each seizure were normalized to the range [0 1], so that the maximum power for each SWD was defined as 1. Finally, the aligned time-frequency dynamics in each channel were averaged across seizures for each subject, and the mean was calculated across subjects.

VI: fMRI Data acquisition

All fMRI data was acquired using the same methods described in Section 2A, Part V.

VII: fMRI Analysis

fMRI data were analyzed using SPM2 software (http://www.fil.ion.ucl.ac.uk/SPM) on a Matlab 7.1 platform (MathWorks, Natick, MA). Images were first realigned to the initial scan of each 10 minute and 40 second functional series. Images were then spatially normalized to the SPM EPI template (in Montreal Neurological Institute or MNI Space). Images were spatially smoothed using a 10 mm full width at half maximum Gaussian kernel. In each 10 minute and 40 second fMRI scanning period, the first 10 image acquisitions (the first 15.5 seconds) were discarded in order to account for initial variations in the scanner's magnetic field. All results for functional data are displayed superimposed on the Montreal Neurological Institute brain template "colin27" (single_subj_T1 in SPM) in radiological convention. Three methods were used to analyze the fMRI data, and their results were compared.

Method 1: Statistical analysis of fMRI data was performed using the general linear model (GLM) approach in SPM2 (50). For each subject, the onsets and durations of SWD periods were identified and used to construct a boxcar model of active (ictal) versus rest (interictal) EEG state. This boxcar function was convolved with the canonical hemodynamic response function (HRF) (51) from SPM2 . The HRF used in this section of the thesis is the has the same parameters as that described in Section 2A, Part V. For

fMRI data obtained during CPT or RTT tasks, 10 minute 40 second periods of task with alternating 32 seconds of CPT/RTT and 32 second periods of fixation was included in the GLM of the periods of SWD in order to remove effects of the behavioral task from BOLD signal changes due to SWD. Both the fMRI data and the design matrices were then high pass filtered at 128 sec, and the resulting model was pre-whitened by an autocorrelation AR(1) model. No global scaling was used in the present analysis. In group analysis, a one sample t-test using a second-order random effects model was performed to determine regions showing significant fMRI changes due to SWD across subjects. We corrected for multiple comparisons using FDR as was described in Section 2A, Part V.

Method 2: Secondly, we performed a model-free, voxel-based analysis of signal changes before, during, and after seizures. This was done by averaging the timecourses of single voxels across subjects. No pre-whitening was performed and the same standard SPM 128 sec high pass filter was used as was describe in the above fMRI analysis method (Section 2A, Part V). The timecourse of fMRI percent change was then calculated for each voxel as $(X1 - X0)/X0 \times 100$, where X1 was signal intensity over time and X0 was averaged signal intensity during entire 10 minute and 40 second scanning period (406 images, after the first 10 images had been removed). This fMRI timecourse was analyzed from 20 seconds before through forty seconds after the onset of each seizure. Periods of SWD were not included if, during the ictal period, subjects did not meet transient movement criteria as described in Section 2A, Part V. Each time course (acquired with 1.55 sec time resolution) was interpolated to obtain values at 0.1sec time

resolution in order to facilitate temporal alignment across data sets. The preictal, ictal, and postictal fMRI time periods were temporally aligned across seizures, and the ictal period of each seizure was scaled to the mean seizure duration (6.6 sec) as described in the EEG analysis of section 2B. Again, the preictal and postictal fMRI data were not scaled, but instead simply aligned by lining up the seizure onset times for preictal data, and by lining up the seizure end times for postictal data. The mean timecourse of each voxel was calculated by averaging across seizures for each subject, and then taking the mean across subjects. Using the resulting mean timecourses, percent fMRI change maps were created for the entire brain at 1 sec intervals that ranged the full pre- (20 seconds before onset) to post-ictal (40 seconds after onset) SWD timecourse. Since CPT/RTT time task blocks were randomly distributed in the analysis and would likely cancel each other out in the mean, CPT and RTT were not included in the model. To estimate any effects of the CPT/RTT tasks on the mean fMRI timecourse, we repeated this analysis using identical data segments relative to task blocks. For each seizure data segment, we identified matching data segments from the same subject with identical duration and identical timing relative to the behavioral task blocks, but during a time when no seizure occurred. The analysis described above was repeated to determine the mean fMRI timecourse in these matching 'no-seizure' data segments.

Method 3: The third fMRI analysis methodology examined specific volumes of interest using MARSBAR (http://marsbar.sourceforge.net/) (52). This analysis further examined the data processed using the voxel-based analysis in the second fMRI analysis method described above. 7 anatomic cortical and sub-cortical volumes of interest (VOI)

were selected based on regions showing the largest fMRI changes in the above, voxel based analysis. VOIs were constructed from the standard MARSBAR regions as follows (Fig. 6): Medial and orbital frontal (Cingulum_Ant + Frontal_Sup_Medial + Frontal_Med_Orb + Frontal_Sup_Orb + Rectus); Lateral frontal (Frontal_Inf_Oper + Frontal_Inf_Tri + Frontal_Mid + Frontal_Sup); Lateral temporal (Heschl + Temporal_Sup); Parietal (Angular + Parietal_Sup + Parietal_Inf + Supramarginal + Cingulum_Post + Cingulum_Mid (posterior half only) + Precuneus); Occipital (Calcarine); Rolandic (Paracentral + Precentral + Postcentral, all truncated below SI 52mm); and Thalamus (Thalamus). The mean timecourse of each VOI for a given fMRI scanning period was calculated by averaging the timecourses of all voxels in this VOI. The percent fMRI change for each VOI mean signal was then calculated as (M1 - M0)/M0 × 100, where M1 was the VOI mean signal intensity over time and M0 was averaged signal intensity during the entire scanning period. As in the voxel-based analysis, we analyzed the time course of each VOI from 20 seconds before the onset of the seizure through 40 seconds after the onset of the seizure, with the same temporal alignment of pre-ictal, ictal and post ictal periods as described in fMRI analysis method 2 above. The mean time course for each VOI was calculated by averaging across seizures for each subject, and then taking the mean across subjects. In order to examine any effects of the CPT/RTT on the mean fMRI timecourse, we again repeated the procedure described above using identical data segments but with no seizures.

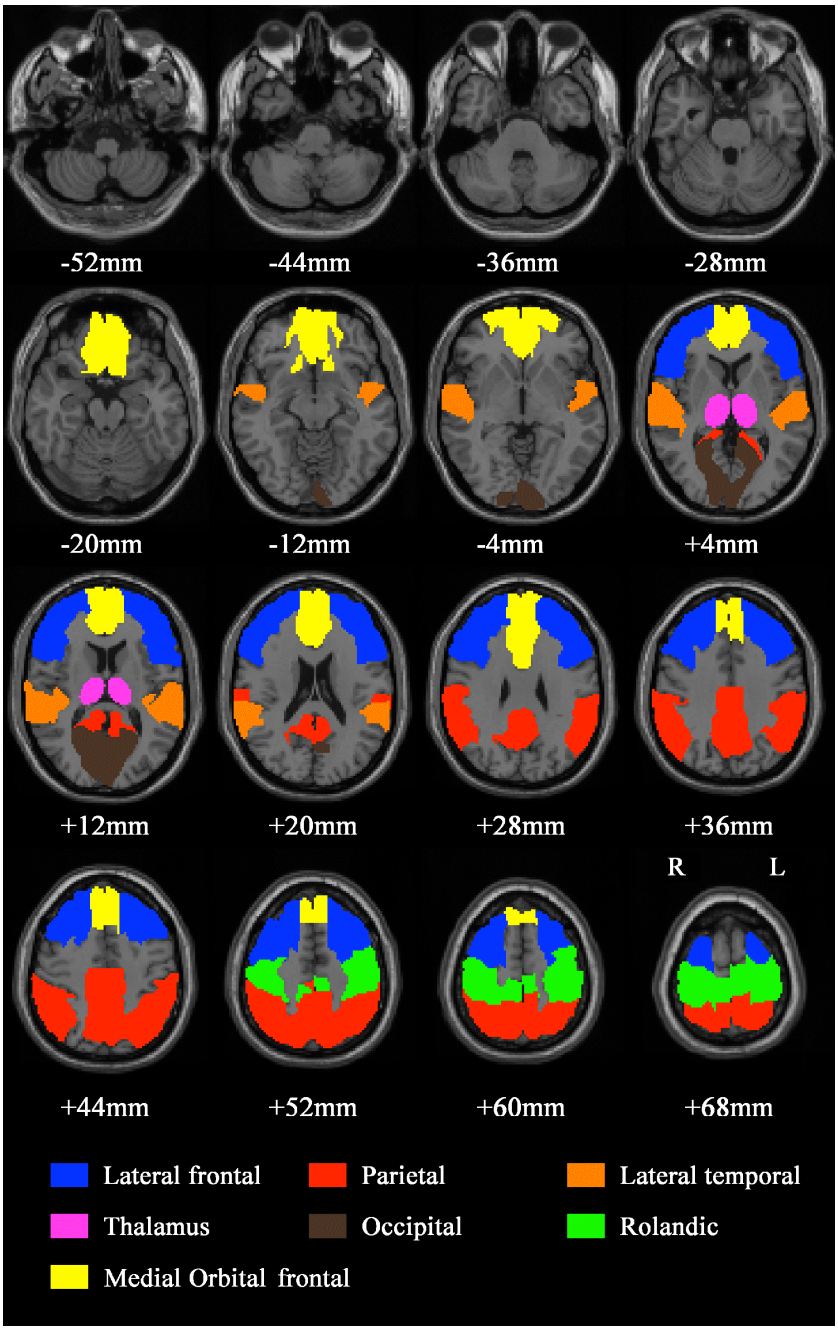

Figure 6. 7 anatomical VOIs chosen based on percent fMRI signal changes observed in Fig. 14, and segmented from SPM MRI template Colin27. VOIs were constructed from the standard MARSBAR regions as follows: Medial and orbital frontal (Cingulum_Ant + Frontal_Sup_Medial + Frontal_Med_Orb + Frontal_Sup_Orb + Rectus); Lateral frontal (Frontal_Inf_Oper + Frontal_Inf_Tri + Frontal_Mid + Frontal_Sup); Lateral temporal (Heschl + Temporal_Sup); Parietal (Angular + Parietal_Sup + Parietal_Inf + Supramarginal + Cingulum_Post + Cingulum_Mid (posterior half only) + Precuneus); Occipital (Calcarine); Rolandic (Paracentral + Precentral + Postcentral, all truncated below SI 52mm); and Thalamus (Thalamus). (Reprinted with permission from Bai, X *et al,* 2010)

Next the fMRI timecourses for the 7 anatomical regions were then compared to each other and to the conventional HRF. Overall shape and timing of fMRI increases were directly compared between the two models of analysis. The amplitude of the canonical HRF obtained from the SPM2 package (in the spm_hrf.m file) was not changed. To evaluate the overall shape and assess the relative contributions of positive and negative components to the fMRI timecourses in each region, we calculated a timecourse polarity index = (Peak amplitude – Trough amplitude)/(Peak amplitude + Trough amplitude). Thus, the timecourse polarity index will be +1.0 for an fMRI timecourse with entirely positive polarity (i.e. a large positive peak without undershoot or other negative trough components), -1.0 for entirely negative polarity, and 0.0 for a bipolar timecourse with equal positive peak and negative trough amplitudes. To statistically compare the early fMRI increases of the 7 VOIs, the positive ½ peak times of the individual subject timecourses were identified and a one-way ANOVA (followed by Tukey's Honestly Significant Difference [HSD] test for post-hoc, pair-wise comparison in SPSS version 15.0) was used to compare these positive ½ peak times across VOIs.

VIII: Author's Involvement

The following experimental procedures in Section 2B were conducted with the express involvement of the author of this thesis: subject recruitment, subject training, subject communication, EEG recording, fMRI acquisition, and behavioral task administration and analysis. Michiro Negishi and Rachel Berman assisted with EEG and fMRI data acquisition, and Xiaoxiao Bai and Hal Blumenfeld conducted the majority of EEG and fMRI analysis in Section 2B.

Chapter 3: Results

3A: Ictal Imaging Results: Simultaneous EEG-fMRI and Behavioral Testing during CAE

I: Absence Seizures

A total of 37 subjects with pure childhood absence epilepsy underwent simultaneous EEG, fMRI, and behavioral testing. 33 of these 37 subjects underwent either CPT, RTT, or a combination of the two behavioral testing tasks. The remaining 4 subjects solely performed Fixation Only scanning periods. 8 subjects performed both types of behavioral scanning (CPT or RTT) as well as Fixation Only scans.

Of the 37 total participants, 9 subjects seized during the fMRI/EEG recording. These 9 subjects had a total of 60 recorded seizures with an average seizure duration of 6.2 ± 4.0 seconds (mean $\pm$ standard deviation). The subjects who seized during the recordings included 6 females and 3 males between the ages of 6 and 15 years and with a mean age of 11.4. The mean age at the time of the participants' first seizure was 8.0 ± 3.0 years (Table 1). All subjects who seized during scanning had been diagnosed with Childhood Absence Epilepsy and had submitted EEGs, performed by non-study-affiliated neurologists, which demonstrated typical 3-4 Hz SWDs with a normal 8 – 10 Hz background.

42 of the 60 seizures were obtained during either CPT or RTT scanning periods. These seizures were recorded from Subjects 1 – 8 (Table 1). Of these 42 seizures, 22 were recorded during the CPT/RTT blocks of the behavioral testing and 20 were recorded during the fixation portion of the CPT/RTT behavioral testing. The remaining 18 seizures were recorded from 4 subjects (subjects 2, 5, 8 and 9) during Fixation Only scanning.

II: fMRI Signal Changes during Absence Seizures

Eight subjects had a total of 42 seizures during CPT and RTT scanning (Table 1, subjects 1 – 8). During these absence seizures, we observed fMRI BOLD signal increases mainly in bilateral thalamus as well as lateral frontal, medial occipital, lateral temporal and superior Rolandic cortices (Fig. 7). We saw ictal BOLD signal decreases in mainly bilateral basal ganglia as well as bilateral parietal and cingulate cortices.

During absence seizures recoded during runs of behavioral testing (i.e. seizures during CPT/RTT and fixation epochs of the CPT/RTT scanning periods), we observed fMRI BOLD signal increases in thalamus (6/8), lateral frontal cortex (6/8 subjects), occipital (primary visual) cortex (6/8), cerebellum (5/8), superior Rolandic (primary somatosensory and motor) cortex (4/8), superior temporal (Heschl's/primary auditory) cortex (4/8), lateral ventricle, and white matter (3/8). Decreases were observed in the lateral parietal cortex (6/8 subjects), medial parietal cortex (precuneus, posterior cingulate) (6/8), basal ganglia (6/8), cerebellum (5/8), anterior cingulate-medial frontal (4/8), and pons (4/8) (Fig. 7).

Interestingly, in addition to the thalamus, many of the changes during seizures involved areas of primary sensory (visual, auditory, somatosensory) and motor (Rolandic) function.

Table 1 Subject CAE clinical information

Sub #	Gender	Age at onset (years)	Age at scan (years)	Medication[a]	EEG[b]	Reported sz frequency at time of onset	Reported sz frequency at time of scans	# Szs during EEG/fMRI[d]	#CPT Runs[c]	#RTT Runs[c]	#Fixation Only Runs[c]
1	F	8	14	Lamotrigine/ none	Normal 8-9 Hz background. Frequent generalized frontal predominant 1.5 to 3.5 Hz spike-wave.	10/day	10/day	1	4	0	2
2	F	11	12	none	Normal 10 Hz background. Frequent generalized frontal predominant 3 Hz spike-wave.	240/day	240/day	9	10	0	8
3	M	6	10	Lamotrigine/ none	Normal 9 Hz background. Bursts of symmetrical large amplitude 3 Hz spike-wave.	1/week	none	3	4	3	0
4	F	4	13	Ethosuximide/ none	Normal 9 Hz background. Frequent generalized frontal predominant 3.5 to 4 Hz spike-wave.	1-2/week	1/week	6	2	2	0
5	M	13	13	none	Normal 9 Hz background. Frequent generalized frontal predominant 3 Hz spike-wave.	15/day	1/day	7	4	4	5
6	F	9	12	Valproate/ none	Normal background of alpha activity with intermixed theta. Frequent generalized 3 Hz spike-wave.	100/day	5/day	3	4	4	0
7	M	10	15	none	Normal 9-10 Hz background. Frequent 3 Hz spike-waves lasing 3-5 sec.	none	none	7	4	4	0
8	F	5	6	none	Normal 7-8 Hz background. Frequent 3-3.5 Hz spike- waves lasing 5-12 sec.	none	5/day	18	5	1	4
9	F	6	8	Ethosuximide/ none	Normal 10 Hz background. Generalized 3 Hz spike-wave lasting 8 sec.	10-50/day	120/day	6	0	0	4

Table 1. [a] Medication being taken before scan / medication at time of scan (see Methods). [b] EEG at time of recruitment obtained from subject clinical EEG records. Similar EEG recordings were obtained for each subject during EEG-fMRI. [c] Scans were repeated on different days for some subjects. Several (up to 6) scanning sessions/runs were performed on each day. [d] Total number of seizures across all scans and runs. Abbreviations: Sub # = Subject Number, sz = seizure

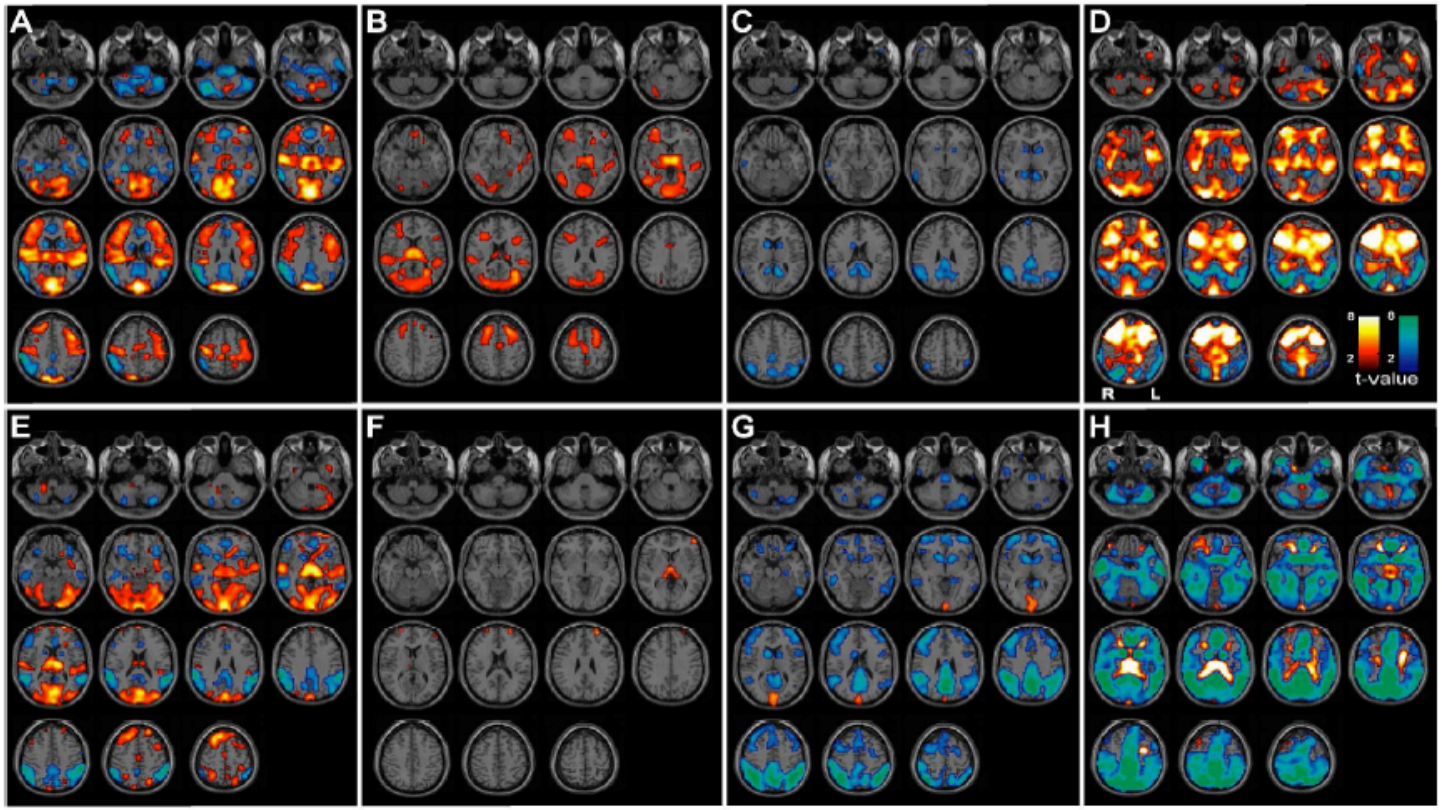

Figure 7. Cortical and subcortical fMRI changes during absence seizures in 8 subjects while undergoing behavioral testing. Axial sections show BOLD fMRI increases (warm colors) and decreases (cool colors) during seizures compared to baseline analyzed in SPM. fMRI increases were seen most consistently in the thalamus, medial occipital, lateral temporal (Heschl's), superior Rolandic, and lateral frontal cortex, and decreases were seen in lateral parietal, medial parietal, cingulate cortex and basal ganglia. **a)** Subject 1, 1 seizure, duration =12.0 sec. EEG of this seizure is shown in Fig. 5b. **b)** Subject 2, seven seizures (mean duration = 4.9 sec). **c)** Subject 3, three seizures (mean duration = 7.8 s). **d)** Subject 4, six seizures (mean duration = 6.0 sec). **e)** Subject 5, six seizures (mean duration = 6.8 s). **f)** Subject 6, three seizures (mean duration = 5.8 s). **g)** Subject 7, seven seizures (mean duration = 2.4 s). **h)** Subject 8, nine seizures (mean duration = 11.4 s). SPM analysis threshold P=0.05, FDR-corrected, & extent threshold k=3 voxels.

To further ensure that none of the above signal changes were due to movement of the subjects within the scanner, we repeated the above analysis after correcting for all degrees of possible motion (3 degrees rotational and 3 degrees translational) during all behavioral scanning periods where seizures were recorded (Fig. 8). No significant differences were observed in the original ictal fMRI signal change patterns after correcting for all possible motion during seizures.

Four subjects had seizures during the Fixation Only periods of behavioral testing (Subjects 2, 5, 8, 9). The ictal BOLD signal changes during these scans are displayed in Fig. 9. The seizure-related, ictal BOLD signal changes in subjects performing Fixation Only (Fig. 9) was remarkably similar to the seizure-related, ictal BOLD signal change in subjects performing either CPT or RTT (Figs. 7 and 8). Again, though now in ictal scanning during Fixation Only, increases were present mainly in the thalamus, occipital, temporal, and frontal cortex, and decreases were seen mainly in the medial and lateral parietal cortex, cingulate, and basal ganglia (Fig. 9).

III: Behavioral Testing Performance during Absence Seizures

This is the first study to evaluate behavioral impairment during absence seizures with simultaneous EEG/fMRI. It has been demonstrated that tasks requiring attentional vigilance and decision making are most severely affected during absence seizures while repetitive tasks are often spared (6, 14, 17). As such, we used the CPT as a task of attentional vigilance in which decision making was required and the RTT as a task requiring repetitive motor responses in order to minimize attentional vigilance.

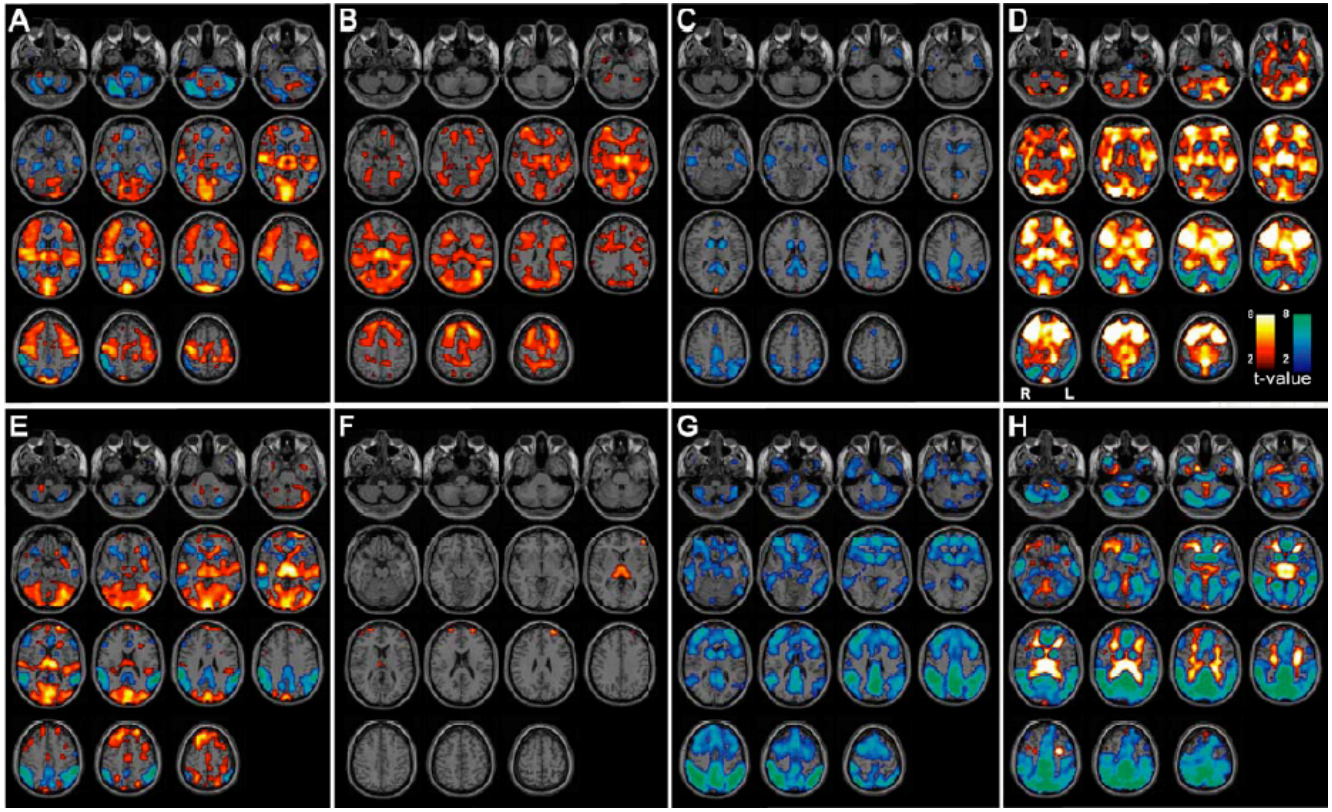

Figure 8. Analysis of seizure-related changes including 6 motion related parameters (3 translation, 3 rotation) in the modeling. Cortical and subcortical fMRI changes during absence seizures appear very similar to the same data without motion-related modeling (Fig. 7). Axial sections show BOLD fMRI increases (warm colors) and decreases (cool colors) during seizures compared to baseline analyzed in SPM. As in Fig 7, fMRI increases were seen most consistently in the thalamus, medial occipital, lateral temporal (Heschl's), superior Rolandic, and lateral frontal cortex, and decreases were seen in lateral parietal, medial parietal, cingulate cortex and basal ganglia. Panels **a) - h)** represent the same individual subjects with the same seizures as in Fig 7. SPM analysis threshold P=0.05, FDR-corrected, and extent threshold k=3 voxels.

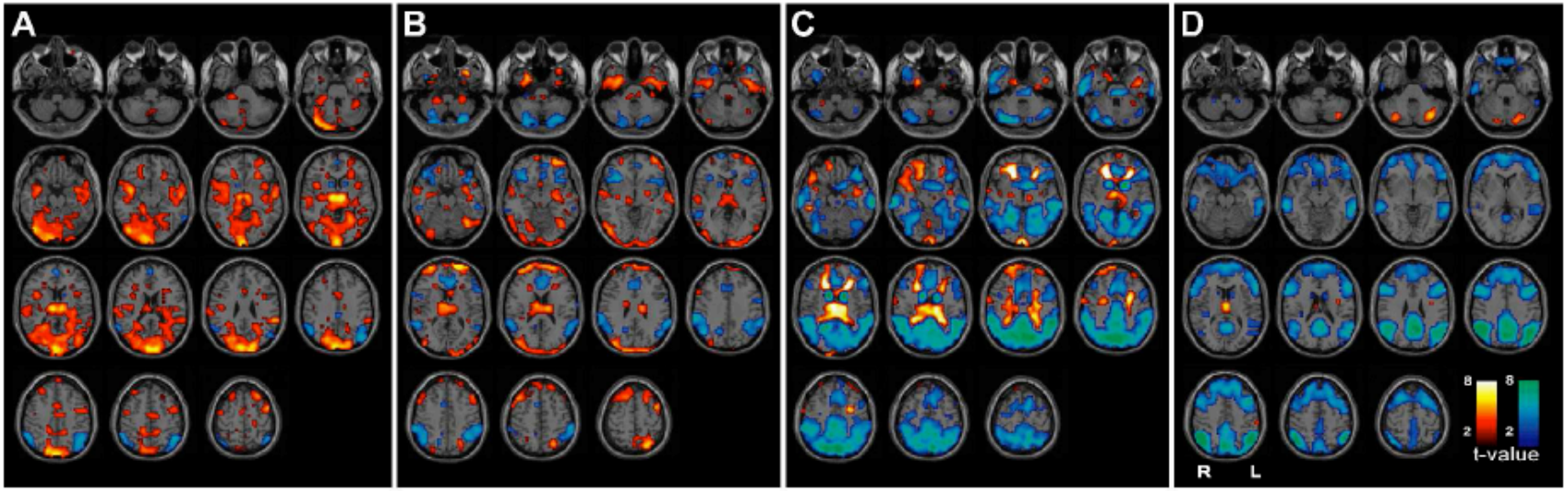

Figure 9. fMRI changes during absence seizures in 4 subjects during Fixation Only (no CPT or RTT). Results were generally similar to fMRI changes in the same subjects with seizures during behavioral tasks (Figs. 7 and 8), showing increases in the thalamus, medial occipital, temporal and lateral frontal cortex, and decreases in the parietal cortex, cingulate gyrus and basal ganglia. Axial sections show BOLD fMRI increases (warm colors) and decreases (cool colors) during seizures compared to baseline analyzed in SPM. a) Subject 2, two seizures (mean duration = 2.3 s). Compare to same subject in Figs. 7b and 8b. b) Subject 5, one seizure (duration = 7.5 s). Compare to same subject in Figs. 7e. and 8e c) Subject 8, nine seizures (mean duration = 7.0 s). Compare to same subject in Figs. 7h and 8h d) Subject 9, 6 seizures (mean duration = 1.9 s). SPM analysis threshold P=0.05, FDR-corrected, and extent threshold k=3 voxels.

42 of the 60 seizures were obtained during either CPT or RTT scanning periods. These seizures were recorded from Subjects 1 – 8 (Table 1). Of these 42 seizures, 22 were recorded during the CPT/RTT blocks of the behavioral testing period and 20 were recorded during the fixation portion of the behavioral testing period. The performance of the subjects on the behavioral tasks during absence seizures are shown in Fig. 10.

As expected, during seizures, subjects performed more poorly on the CPT task. The omission error rate for the CPT was defined as the number of missed targets (i.e. X presentations when the subject failed to press the button) divided by the total number of target presentations. Omission rate for RTT was defined as the number of missed targets (i.e. any time the subject did not press the button in response to any letter) over the number of targets presented. CPT omission rate during absence seizures was 81% (13/16) and RTT omission rate during seizures was 39% (24/60) ($\chi^2 = 8.60$; $p<0.003$). Interictal CPT and RTT omission rates were generally below 10 % and composed a negligible percentage of total interictal target presentations.

These omission error rates were similar to those previously reported using similar ictal behavioral tasks in subjects with CAE without fMRI. These error rates also support findings that, during absence seizures, subjects with CAE perform worse on tasks requiring attentional vigilance than they do on tasks requiring repetitive motor performance (6, 14, 17). This finding also lends evidence to the fact that the seizures observed during the simultaneous EEG/fMRI recording were absence seizures with behavioral impairment and not simply SWD without behavioral effects.

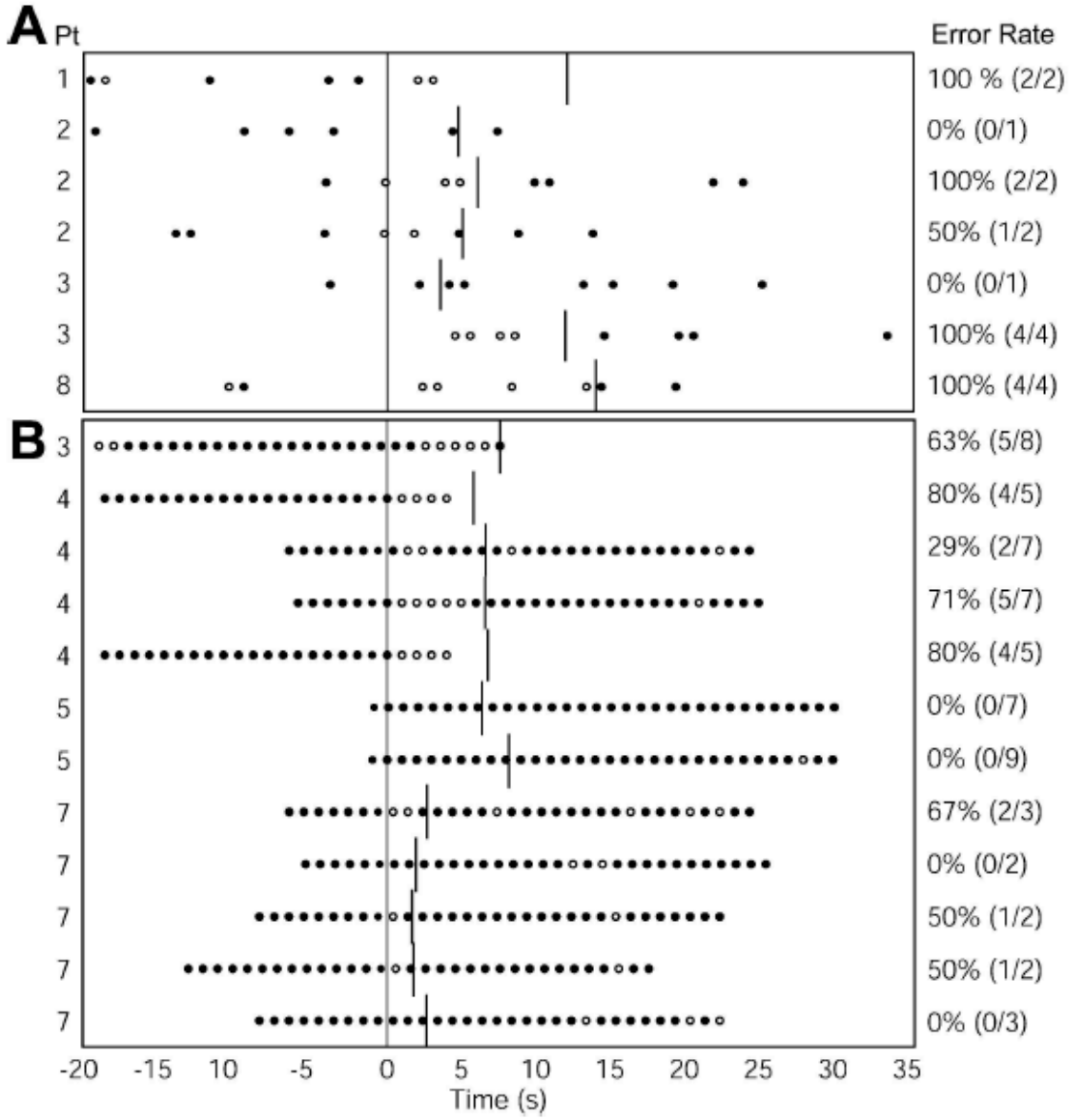

Figure 10. Behavioral performance on CPT and RTT tasks during absence seizures. Behavioral tasks consisted of 32 sec blocks of letter presentations, alternating with 32 sec epochs of fixation. Letters were presented once per second. a) For CPT, the target (X) occurred at random, at an average rate of once per 4 seconds. Mean omission error rate during seizures was 81%.(13/16). b) During RTT, patients were instructed to push the button for all letters (no Xs were presented). Mean omission error rate during seizures was 39% (24/60). ● = correct response to target. ○ = omission error. Symbols appear at time of letter presentation. Response was required within 1000 ms of letter presentation. Vertical line at t = 0 is seizure onset. Other vertical lines denote seizure end. 22 seizures were recorded during task blocks, but two seizures had no target letters occurring during the spike-wave discharge, and one could not be analyzed due to technical difficulty with button press recording, resulting in 19 seizures total. Pt = Subject number.

Additionally, the SWD observed during the simultaneous EEG, fMRI, and behavioral testing demonstrated other previously reported characteristics of absence seizures. Notably, seizure frequency was markedly less during tasks requiring attentional vigilance (6). Only 16 seizures, or an average of 2.7 seizures per hour of testing, were observed during the CPT task whereas 60 seizures, or 6.8 seizures per hour of testing, were observed during the RTT task ($p = 0.05$).

It is also important to note that, similar to previous studies (6), behavioral performance was variable during the SWD observed in this study. In other words, within a single subject tested, a SWD in one instance could disrupt performance on a behavioral task, while a separate SWD, at a different time of scanning, though of similar duration and quality and in the same subject, could spare behavioral performance (egg Fig. 10, Part A, Subject 2). Again, this characteristic finding supports the notion that the SWD observed in this study, during simultaneous EEG/fMRI, were typical absence seizures with characteristic ictal behavioral disturbances normally seen in the CAE population.

3B: Ictal Timecourse Results : Timecourse of fMRI and behavioral changes during typical childhood absence seizures

I: Absence Seizures

A total of 42 subjects with pure CAE underwent simultaneous EEG, fMRI, and behavioral testing (CPT and RTT), and 9 of the subjects had SWD during their scanning sessions. Of these 9 subjects (3 male and 6 female), the mean age at time of study was 11.9 years with a range from 6 to 15 years of age. The mean age at the time of first seizure in the 9 subjects was 8.1 years with a range from 4 – 13 years of age.

These 9 subjects had a total of 88 recorded seizures with an average seizure duration of 6.6 sec. 74 of these seizures were obtained during CPT or RTT scanning periods. Fixation Only scanning was performed in 4 of the 9 abovementioned subjects and accounted for 14 of the 88 recorded seizures.

In analyzing the data, attempts were made to include as many SWD episodes as possible. In the behavioral analysis, though, some seizure episodes had to be eliminated, however, due to lack of behavioral testing (no target letter presentation during seizure), ictal movement greater than the abovementioned acceptable parameters, or insufficient time between seizures to allow for adequate timecourse analysis (i.e. seizures where the pre-ictal period from one seizure overlapped with the post-ictal period of the preceding seizure). In total, 53 of the 88 seizures from 8 of the 9 subjects were included in behavioral analysis. 41 of these seizures were in CPT scanning periods and 12 in RTT periods.

For EEG and fMRI analysis, we were able to use 54 of the 88 seizures (9 subjects). Of these seizures, 40 occurred in 8 subjects during CPT or RTT scanning

sessions and 14 occurred in 4 subjects during Fixation Only scanning sessions. 3 subjects had seizures during both behavioral testing periods (CPT/RTT) and Fixation Only scanning periods. The same 54 seizures were used for both EEG and fMRI analyses with the exception of the exclusion of 3 seizures from 1 subject in the fMRI voxel-based and VOI analyses. These seizures were excluded from fMRI analyses methods 2 and 3 (above) because transient movement occurred either in the pre- or post-ictal period. This movement was sufficiently distant from the ictal period though, and therefore these seizures could be analyzed with the conventional GLM analysis (50).

In summary, 54 seizures (8 subjects) were used for EEG and GLM fMRI analysis, 53 seizures (8 subjects) for behavioral analysis, and 51 seizures from 8 subjects for voxel-based and VOI fMRI analyses. In total, the seizure data included across analyses was practically identical and certainly sufficient to allow between-group comparison.

II: EEG Timecourse

The changes in EEG signal and frequency power was tightly temporally-locked to the beginning and the end of seizures (Fig. 11). All 54 seizures demonstrated frontally-predominant SWDs and, as such, we used the above Fourier Transform to calculate the frequency dynamics of the SWDs. Fig. 11 displays a plot of average frequency power of the F7 electrode in all 54 SWDs from 20 seconds before the onset to 26 seconds after the onset of the SWDs. Results of similar frequency power plots using other channels (F3, F4, FP1, FP2, and F8) across the 54 SWD were quite similar to Fig 11 and are not

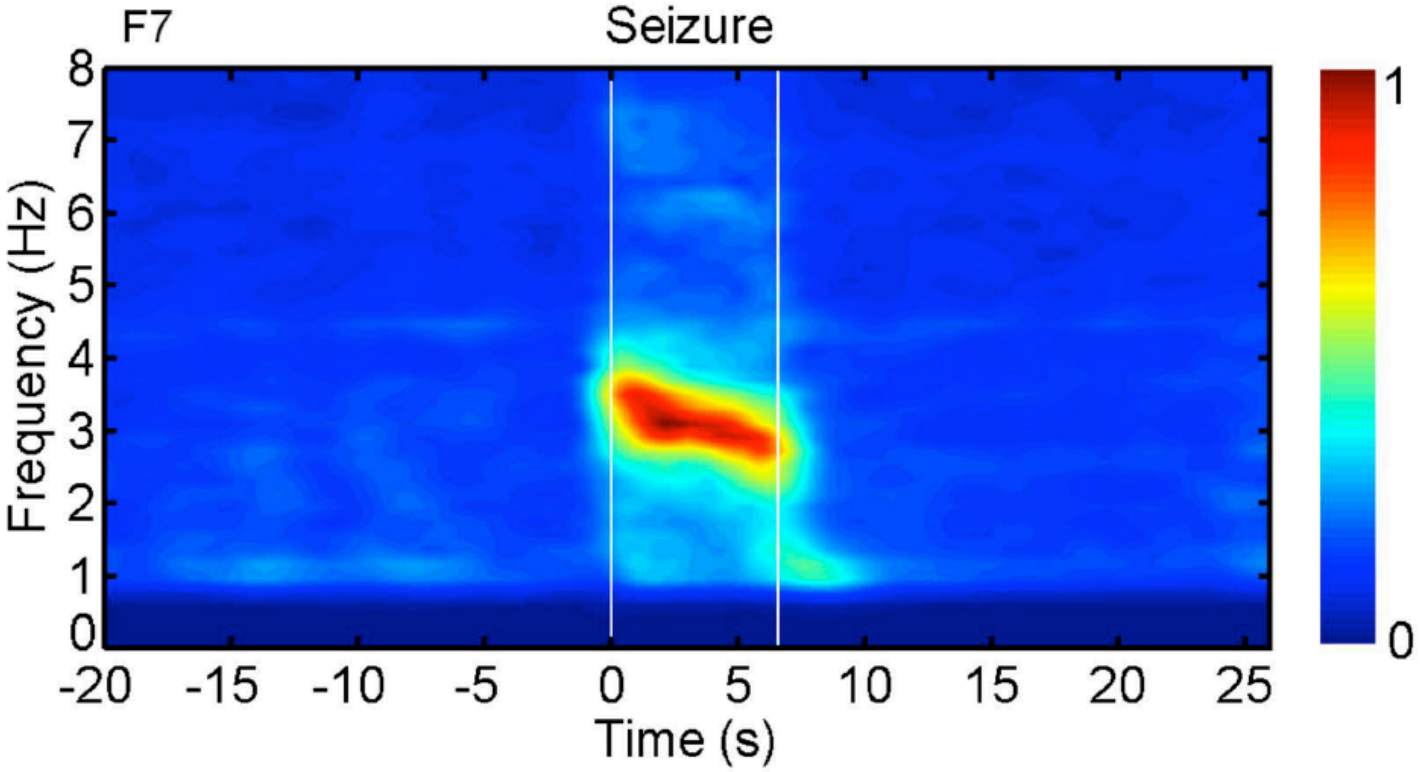

Figure 11. EEG signal power changes abruptly at beginning and end of seizures. Average time-frequency dynamics of spike-wave discharges in channel F7 from -20 sec to +26 sec relative to seizure onset. A total of 54 seizures (9 subjects) were analyzed: 40 seizures in 8 subjects during CPT or RTT; 14 seizures in 4 subjects during Fixation Only. Analysis was performed by using short-time Fourier transform (see section 3B). All ictal periods were scaled to the mean seizure duration (6.6s); and the preictal (-20 to 0 sec), ictal (0 to 6.6 sec), and postictal (seizure end to +26 sec) periods were then temporally aligned across seizures. The power spectrum was normalized to a range of [0 1] and shown in blue to red scale where the maximum power for each seizure in the range 0 to 25 Hz from -20 sec to +26 sec was defined as "1". Power-frequency maps for all seizures were averaged across patients. The dominant frequency component of the EEG signal was 3~4Hz, which was only observed during spike-wave discharges. (Reprinted with permission from Bai, X *et al,* 2010)

displayed here. As expected with SWD typical of CAE, the dominant frequency component was in the 3 – 4 Hz range, seeming to begin more in the 4 Hz range at seizure onset and slow to the 3 Hz range by the end of the ictal period.

III: Timecourse of Behavioral Changes

Like changes in EEG signal power, behavioral impairment was tightly correlated with both the beginning and end of the observed seizures (Fig. 12).

In CPT, percent correct responses dropped rapidly from 98% to 38% three seconds before the onset of SWD. Interestingly CPT performance was consistently impaired even before the electrographic onset of the SWD. During seizures, percentage correct rates in the CPT task were even lower, at 0%, 6% and 21% in the consecutive ictal time bins. Within 2 seconds of the average seizure end time, CPT responses had recovered to baseline (97%).

Performance on RTT was less impaired during seizures than CPT performance. RTT impairment began later, on average, than in CPT and was, overall, less profound. RTT percent correct responses were only affected during the electrographic SWD, and were 72%, 39% and 65% during the ictal period. Interictal CPT and RTT omission rates were generally below 10 % and composed a negligible percentage of total interictal target presentations. In our results, the fluctuation in both baseline CPT and RTT performance are likely due to the variable and small sample sizes in some bins, although potential pre- and post-ictal deficits can not be excluded.

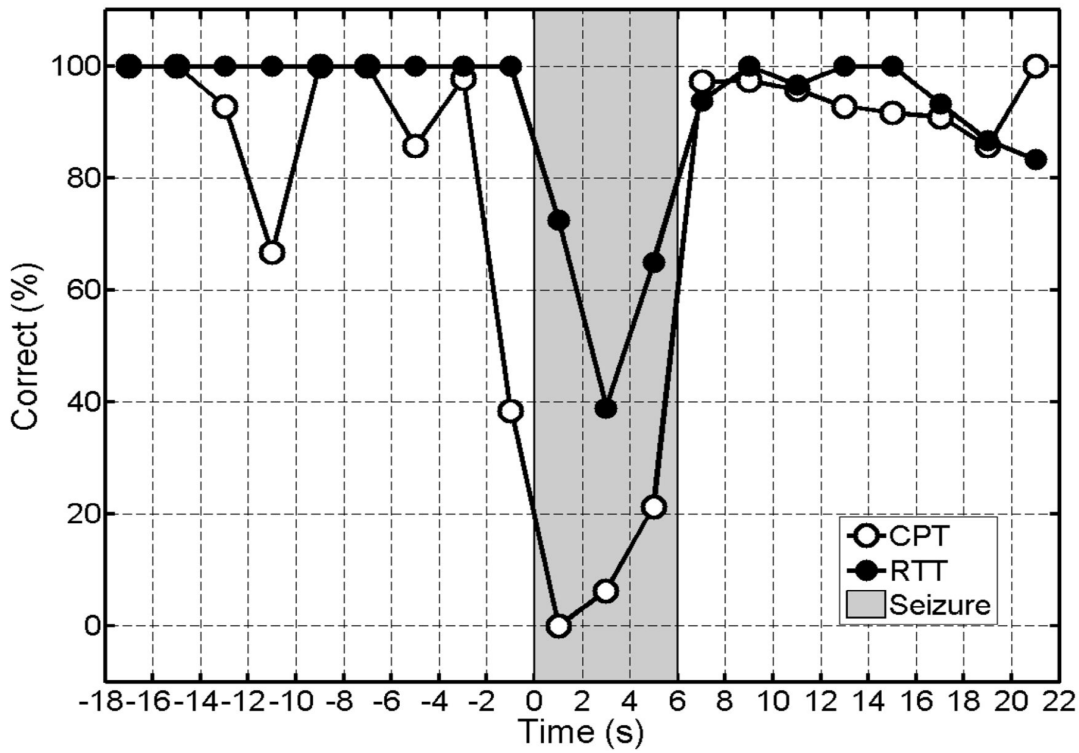

Figure 12. Behavioral impairment during seizures. Percent correct responses are shown over time (2 sec time bins) before, during and after seizures (shaded region). Data were temporally aligned to match the pre-ictal, ictal, and post-ictal periods across seizures as described in the text. Performance on the CPT task declined rapidly for letters presented just before seizure onset and recovered quickly after seizures end. Impaired performance on the RTT task was more transient than on CPT, did not begin until after seizure onset, and was less severely impaired during seizures than the CPT task ($F = 15.3$, $P = 0.017$; ANOVA). Results are based on a total of 53 seizures in 8 patients; 41 seizures in 5 patients during CPT and 12 seizures in 4 patients during RTT. Fluctuations in baseline with CPT appear due to variable and small sample sizes in some CPT bins (e.g. -12 to -10s bin), since target letters appear on average only once per 4 seconds with CPT, while they appear every second with RTT. (Reprinted with permission from Bai, X *et al,* 2010) (53)

CPT percentage correct responses, in the bin before seizure onset as well as the three bins during SWD, were significantly worse ($F = 73.6$, $P < 0.001$ on ANOVA with post-hoc, pair-wise Tukey HSD) than RTT ($F= 16.3$, $P = 0.001$) at each respective time point. Of note, the deficits evident in the CPT bin directly before seizure onset likely reflect an ictal deficit and not a true pre-ictal deficit, as these pre-ictal stimuli were presented so close to the onset of SWD that mean response time (502.9 msecs across all subjects in all CPT periods) would, on the whole, have put the button press response to the target presentation well within the ictal period.

IV: Ictal fMRI Analysis using Standard Hemodynamic Response Function and General Linear Modeling

This method of analysis, currently commonplace in previous studies of ictal fMRI in CAE (18, 21, 24, 26), examines the ictal BOLD signal changes assuming these changes are governed by a standard hemodynamic response function (51) and that they abruptly begin and end in close temporal association with the SWD on EEG (50).

The results of this analysis are demonstrated in Fig. 13, and are consistent with the findings of the previous work that rested upon similar assumptions (18, 21, 24-26). As demonstrated in Fig. 13, we observed fMRI BOLD signal increases mainly in bilateral thalamus and medial occipital cortex with decreases in “default mode areas” of bilateral lateral parietal cortex, precuneus, anteroventral basal ganglia, and cingulate gyrus.

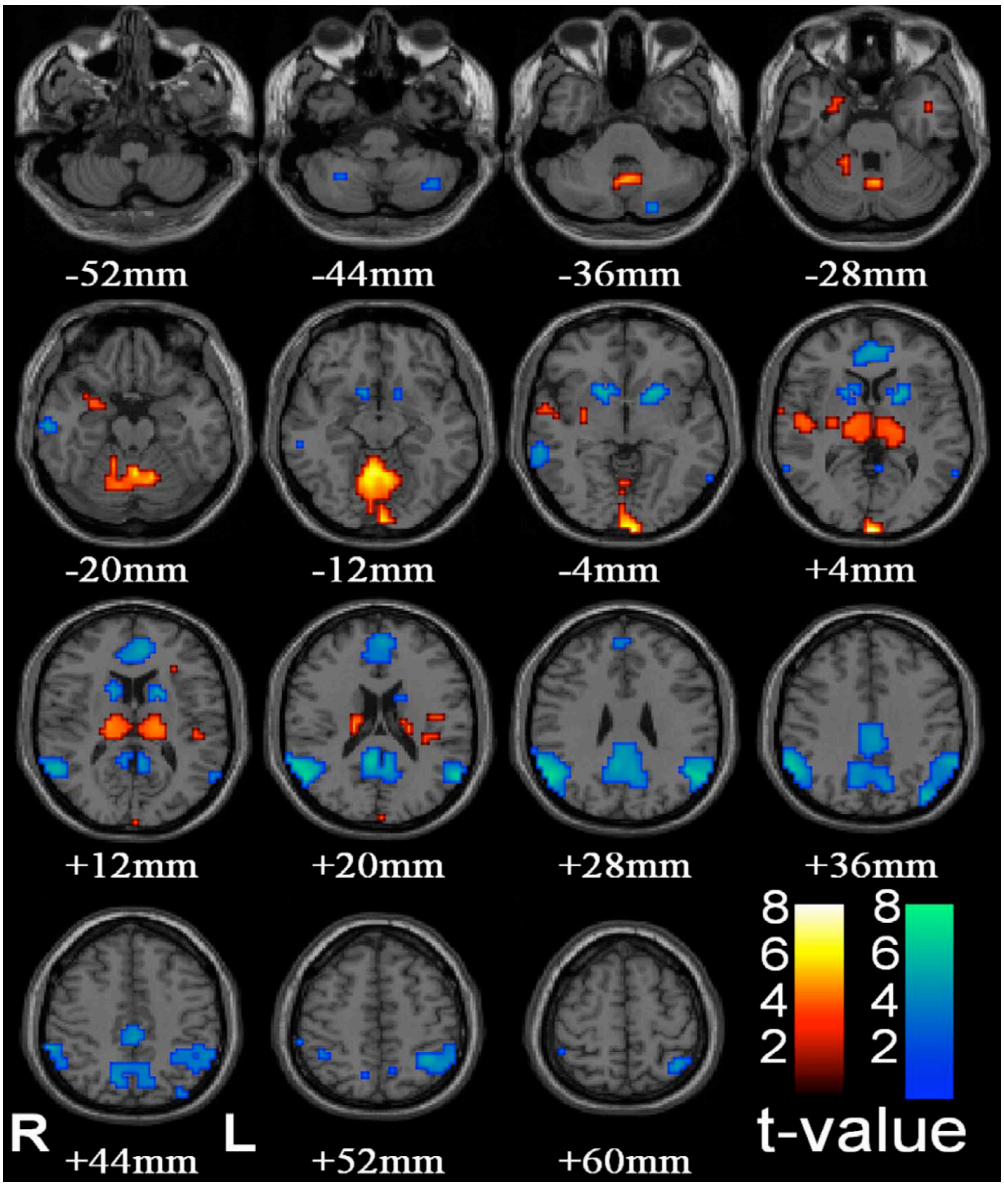

Figure 13. Thalamic increases and "default mode" cortical decreases are the most prominent changes seen with conventional HRF modeling in SPM. fMRI increases (warm colors) and decreases (cool colors) are shown resulting from group analysis with second level random effects analysis, FDR-corrected height threshold $p < 0.05$, and extent threshold $k = 3$ voxels (voxel dimensions = 2×2×2mm). Functional data are superimposed on the Montreal Neurological Institute brain template "colin27" (single_subj_T1 in SPM2) displayed in radiological convention. In total, 54 seizures in 9 subjects (40 in 8 subjects during CPT or RTT; 14 in 4 subjects during Fixation Only, 3 subjects with both CPT/RTT and Fixation Only runs) were analyzed using GLM with canonical HRF in SPM2. fMRI increases were seen in bilateral thalamus, occipital (calcarine) cortex, and to a lesser extent the midline cerebellum, anterior and lateral temporal lobes, insula, and adjacent to the lateral ventricles. fMRI decreases were seen in the bilateral lateral parietal, medial parietal, cingulate cortex and basal ganglia. (Reprinted with permission from Bai, X *et al,* 2010)

V: Ictal fMRI Timecourse Analysis using Voxel-Based Percentage Change

This method of analysis used the more data-driven approach explained above. Different from the general linear model of fMRI analyses (50), this voxel-based percentage change approach does not assume that fMRI activity is related to underlying brain activity via the Glover, standard HRF model (51). This model also does not assume that fMRI activity begins and ends with the abrupt onset and offset of SWD on EEG. Instead, this method of analysis assumes no fMRI signal variation based on the traditional HRF and simply examines mean percentage signal change on a second-by-second basis, before, during and after the onset of SWD on EEG.

As demonstrated in Fig. 14, this data-driven method of analysis reveals changes in fMRI signal that could not possibly be observed using the previous GLM. In this voxel-based timecourse model, fMRI signal is observed to increase in some areas of the brain as early as 8 to 14 seconds before the electrographic onset of seizure and last until up to 24 seconds after seizure onset, well after the electrographic seizure had disappeared. These fMRI BOLD signal increases are seen first in bilateral medial orbital frontal cortex, followed by bilateral frontal polar cortex, bilateral cingulate cortex, and bilateral lateral occipital cortex. During the 6.6 second mean duration of the seizure, increases are seen in bilateral temporal and lateral frontal cortices. After the end of SWD on EEG, positive changes in fMRI BOLD signal continue to arise; next in the bilateral medial occipital cortices and finally in the bilateral thalami, up to 8 seconds after the disappearance of SWD.

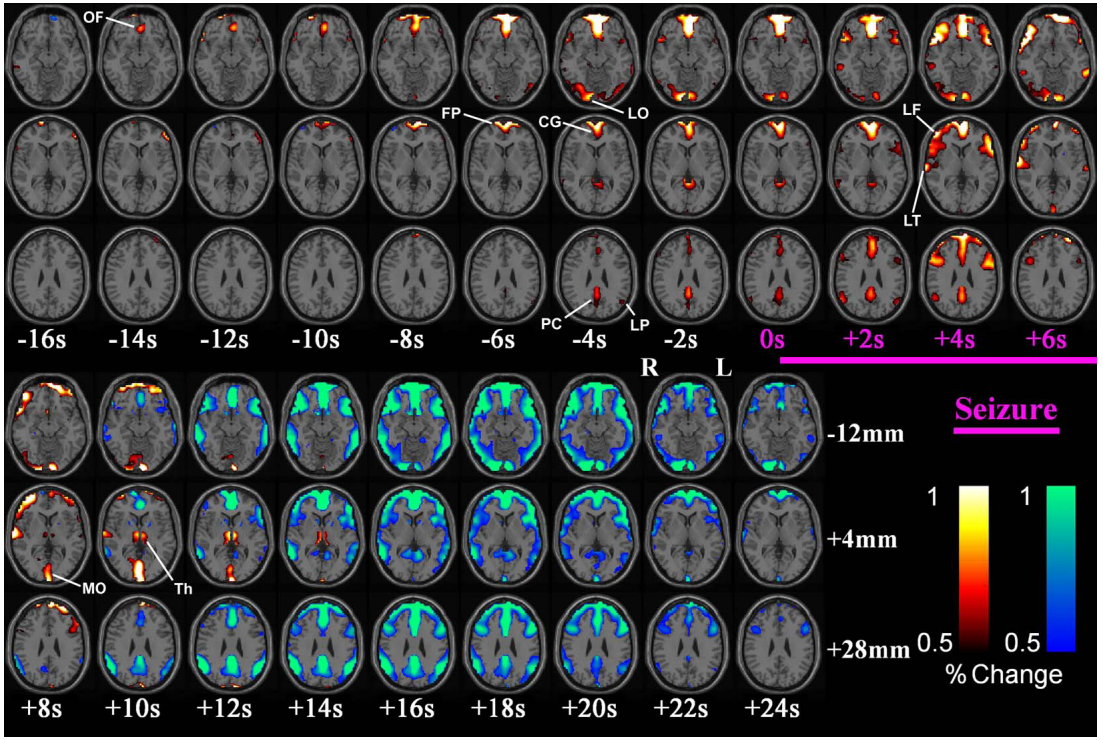

Figure 14. Early and late fMRI changes in cortical-subcortical networks associated with absence seizures. Percent fMRI signal changes are shown from group analysis of patients described above (methods). fMRI percent change increases (warm colors) and decreases (cool colors) are shown, with a display threshold of 0.5%. The ictal time period of seizures was scaled to 6.6s (mean seizure duration), and the preictal, ictal, and postictal time periods temporally aligned across all seizures. Early fMRI signal increases were seen well before seizure onset (0s) in medial orbital frontal (OF), frontal polar (FP), cingulate (CG), lateral parietal (LP), precuneus (PC), and lateral occipital (LO) cortex. After seizure onset, fMRI increases progressed to also involve lateral frontal (LF) and temporal (LT) cortex. Following the end of seizures, fMRI increases were seen in the medial occipital (MO) cortex, and lastly in the thalamus (Th). fMRI signal decreases occurred later, and continued well after seizure end. Decreases were observed initially in medial/orbital frontal, cingulate, medial and lateral parietal cortex, followed by decreases in lateral frontal, temporal and occipital cortex, and basal ganglia. (Reprinted with permission from Bai, X *et al,* 2010)

fMRI decreases in BOLD activity are not seen, using this voxel-based percentage change model, until after SWD cease. These decreases are first seen in the seconds after electrographic offset of SWD and begin in medial/orbital frontal, cingulate, and medial and lateral parietal cortices and continue, up to 18 seconds after EEG seizure offset, in lateral frontal, temporal, and occipital cortices as well as basal ganglia.

As noted above, behavioral testing did occur during various portions of time displayed in Fig. 14, and this behavioral testing was not accounted for in this voxel-based, percentage change model. To control for this, in Fig. 15, we used the same voxel-based percent change analysis to examine periods of testing that differed from those displayed in Fig. 14 only in that subjects during the periods of time included in Fig. 15 did not have seizures. As demonstrated in Fig 15, without seizures and with identical periods of behavioral testing, we observed minimal cortical or sub-cortical changes in fMRI BOLD signal. This suggests that signal change due to random periods of behavioral testing in Fig. 14 averaged out, leaving bold signal changes that are specifically associated with absence seizures.

VI: Ictal fMRI Timecourse Analysis using Volumes of Interest

In order to determine if the standard HRF (51) adequately correlated with the fMRI changes seen in specific regions of the brain, we calculated percentage fMRI change maps for volumes of interest (VOI) (Fig 16) and compared them to the expected standard HRF model (51). If fMRI signal changes as predicted by the standard HRF convolved by the a boxcar function representing seizure duration, then all fMRI changes

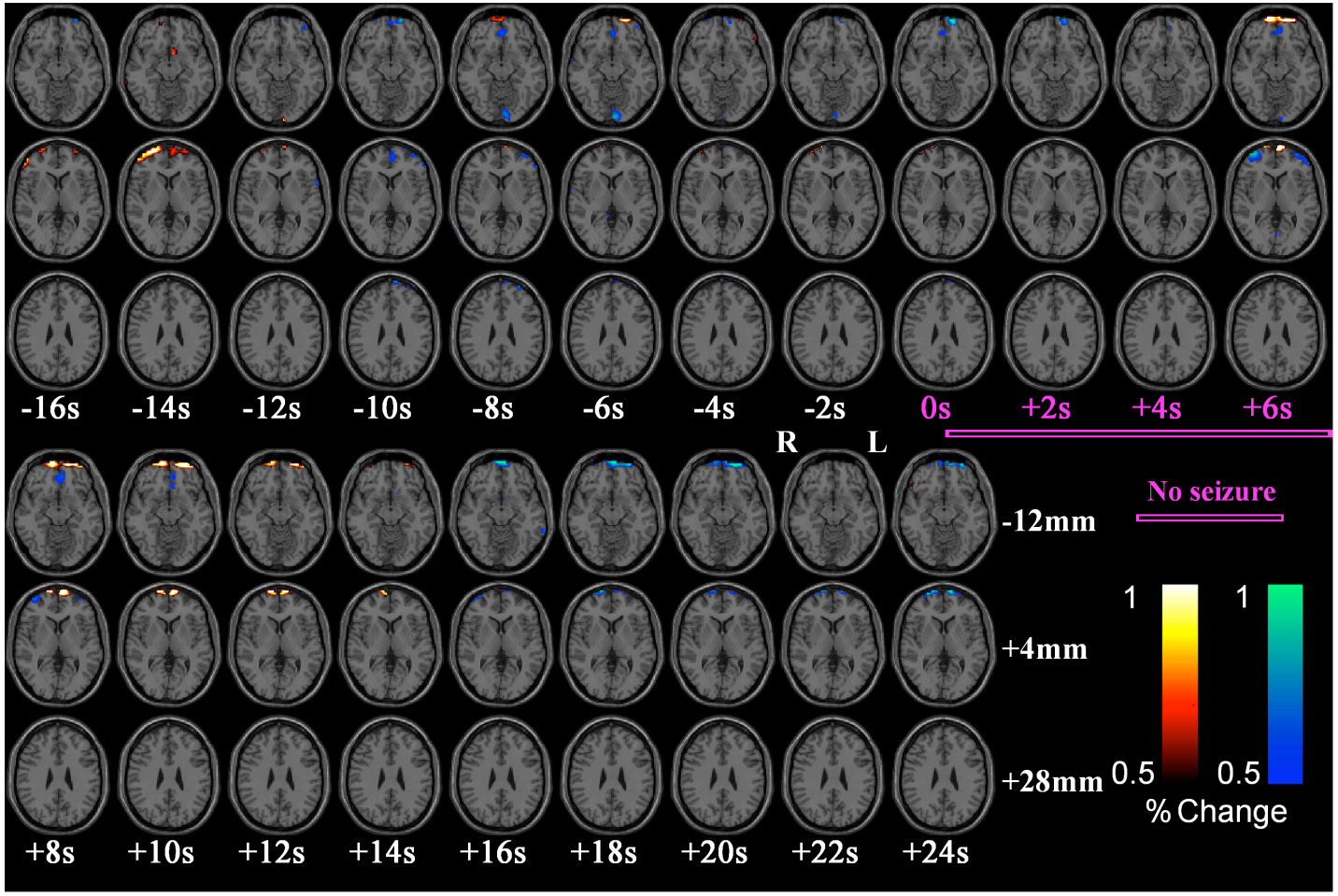

Figure 15. Cortical and subcortical fMRI percent change maps during no seizure periods of identical behavioral testing . We performed a group analysis using the same number of data segments, with identical timing with respect to behavioral tasks, and from the same patients as Fig 14, but during times when no seizures occurred. fMRI percent change increases (warm colors) and decreases (cool colors) are shown, with a display threshold of 0.5%. (Reprinted with permission from Bai, X *et al,* 2010)

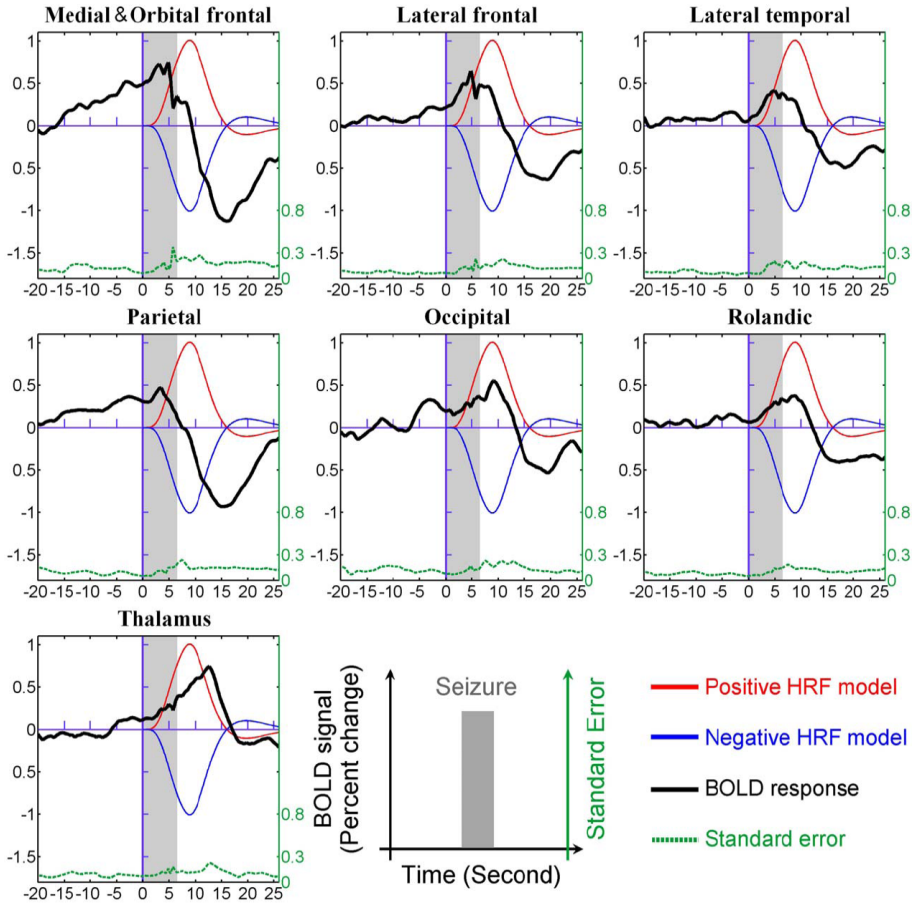

Figure 16. fMRI timecourses during absence seizures differ substantially from the Glover model HRF in most regions. Mean fMRI timecourses in 7 anatomical VOIs (see Figs 6 and 14) are shown from -20 sec to +26 sec relative to the seizure onset. Red and blue curves represent the positive and negative HRF models obtained by convolving a boxcar function of 6.6 sec (mean seizure duration, shown in gray) with the canonical HRF of SPM2. Data used for the generation of this figure are the same as in Fig. 14, and were obtained from group analysis of 51 seizures in 8 subjects. (Reprinted with permission from Bai, X *et al,* 2010).

should begin after seizure onset, have a large positive peak at 9 sec, followed, 10.8 seconds later, by a slightly negative trough (Fig. 16, red curves). Regions showing decreases predicted by the Glover HRF model are simply predicted to have the inverse of the typical positive HRF (Figure 16, blue lines). The standard Glover model predicts fMRI increases will have a polarity index of +0.81 and decreases a polarity index of –0.81 (Table 2) (51).

As several regions demonstrated large percentage change associated with seizures in Fig. 14, we examined these regions (orbital/medial frontal, lateral frontal, parietal [lateral + precuneus], lateral temporal, occipital, and Rolandic cortices and the thalamus) using volumes of interest (See Fig. 6). The percentage change maps for each of these areas are displayed in Fig 16. None of these percentage change maps resembled the increases or decreases predicted by the traditional Glover HRF, with the exception of perhaps the thalamus (51). Though there was variation in the shape and size of the other percentage change maps across VOIs, each of the fMRI timecourses demonstrated a pre-ictal positive fMRI signal change, followed by a fMRI signal decrease and then by a return to baseline.

In order to better characterize the timecourses of each VOI, we calculated ½ peak times across regions (Table 2). As noted in Fig. 14, the first ictal increases were seen in parietal and orbital frontal regions with respective ½ peak times of 6.6 and 4.9 seconds before SWD onset. This was followed by ½ peak times of +1.8 sec in the lateral frontal and +2.4 sec in the lateral temporal regions. Finally, the Rolandic, occipital, and thalamus showed ½ peak times of +3 sec, +4.5 sec, and +6.5 sec, respectively. Generally, fMRI decreases (½ trough times) showed the same sequence as fMRI ½ peak times (Table 2).

Table 2: Timing and shape of fMRI percent change timecourses for HRF model vs. VOI-based data.

	1/2 Peak Time	Peak Time	1/2 Trough Time	Trough Time	Timecourse Polarity Index[b]
HRF Model, Positive[a]	5.3	9	17.1	19.8	0.81
HRF Model, Negative[a]	17.1	19.8	5.3	9	-0.81
Parietal	-6.6	3.5	10.5	15.2	-0.25
Orbital/medial frontal	-4.9	4.8	11.4	15.9	-0.20
Lateral frontal	1.8	4.8	13.4	19.3	0.01
Lateral Temporal	2.4	4.9	13.3	18.2	-0.04
Rolandic	3	8.8	13.5	17.2	-0.02
Occipital	4.5	9.1	14.6	19.4	0.01
Thalamus	6.5	12.7	17.6	21	0.36

[a]Positive and negative HRF models are inverted but otherwise identical

[b]Timecourse polarity index = (Peak amplitude – Trough amplitude)/(Peak amplitude + Trough amplitude).

When comparing the individual VOI's ½ peak times using ANOVA with post-hoc Tukey's HSD, there is a significant difference between the 7 regions ($F = 3.78$, $p = 0.003$). Additionally, the ½ peak time for medial/orbital frontal ($p = 0.005$) and parietal ($p = 0.021$) regions were significantly earlier than the thalamus. The medial/orbital frontal cortex ½ peak time was also significantly earlier than the temporal VOI ½ peak time ($p = 0.036$) (Table 2).

Illustrative of the differences seen between GLM and voxel-based percentage change VOI modeling, both the parietal and orbitofrontal cortex showed early increases in VOI modeling (Fig. 16), and show mainly decreases in the GLM model (Fig. 13). This is because the late decreases in both the medial/orbital frontal and parietal regions most closely resemble the Glover HRF predicted fMRI signal decreases (i.e. blue curves in Fig. 16) in the GLM and therefore show up as only decreases on the GLM. These large fMRI signal percentage changes in the medial/orbital frontal and parietal regions also have timecourse polarity indexes of -0.2 and -0.25 respectively. These timecourse polarity indexes most closely resemble the timecourse polarity index for the negative HRF model (i.e. Glover model for HRF decreases) (Table 2) (51).

Additionally, the percentage fMRI signal change timecourses for the lateral frontal and lateral temporal VOIs have largely neutral polarity indexes (0.01 and 0.04 respectively, Table 2) and cross the zero level at roughly the point of Glover positive HRF peak (red curves, Fig. 16) (51). Therefore, the ictal fMRI signal changes displayed in the conventional GLM using Glover HRFs (Fig. 13) largely mask the fMRI signal timecourses in these two areas.

The occipital and Rolandic timecourses are similar to the lateral frontal and lateral temporal timecourses in that they all have a biphasic shape and resultant polarity indexes close to the zero level (Fig. 16, Table 2). The occipital and Rolandic timecourses, however, are different from the largely GLM-invisible lateral frontal and lateral temporal fMRI changes in that the occipital and Rolandic timecourses are shifted earlier in time with respect to seizure onset and, thus, most closely resemble the positive Glover HRF (Fig. 16). As such, the occipital VOI is represented as having fMRI signal increases on GLM analysis (Fig. 13). In our analysis, Rolandic fMRI increases were below the significance threshold on our GLM model (absent in Fig. 13), however, have been reported to demonstrate fMRI signal increases in prior SPM studies of ictal fMRI in CAE subjects (18, 20, 24, 26, 27).

Finally, the thalamus, most resembling the traditional positive HRF model (Fig. 16), and, with a similar polarity timecourse index of 0.36 (Table 2), is notably displayed as demonstrating strong increases in signal when ictal fMRI is modeled using the GLM (Fig. 13).

The VOI timecourse analysis used to generate Fig. 16 also contained uncontrolled-for, random distributions of behavioral task performance. Similarly to the voxel-based timecourse analysis in Fig 15, we repeated the VOI timecourse analysis using identical segment timing but using segments without seizures in order to examine the effect of the behavioral task alone (without seizures) (Fig. 17). As in Fig. 15, there were hardly any fMRI signal changes in this model, strengthening the assertion that the timecourse of fMRI signal change demonstrated in VOI analysis (Fig. 16) was due to ictal fMRI changes rather than other confounding factors.

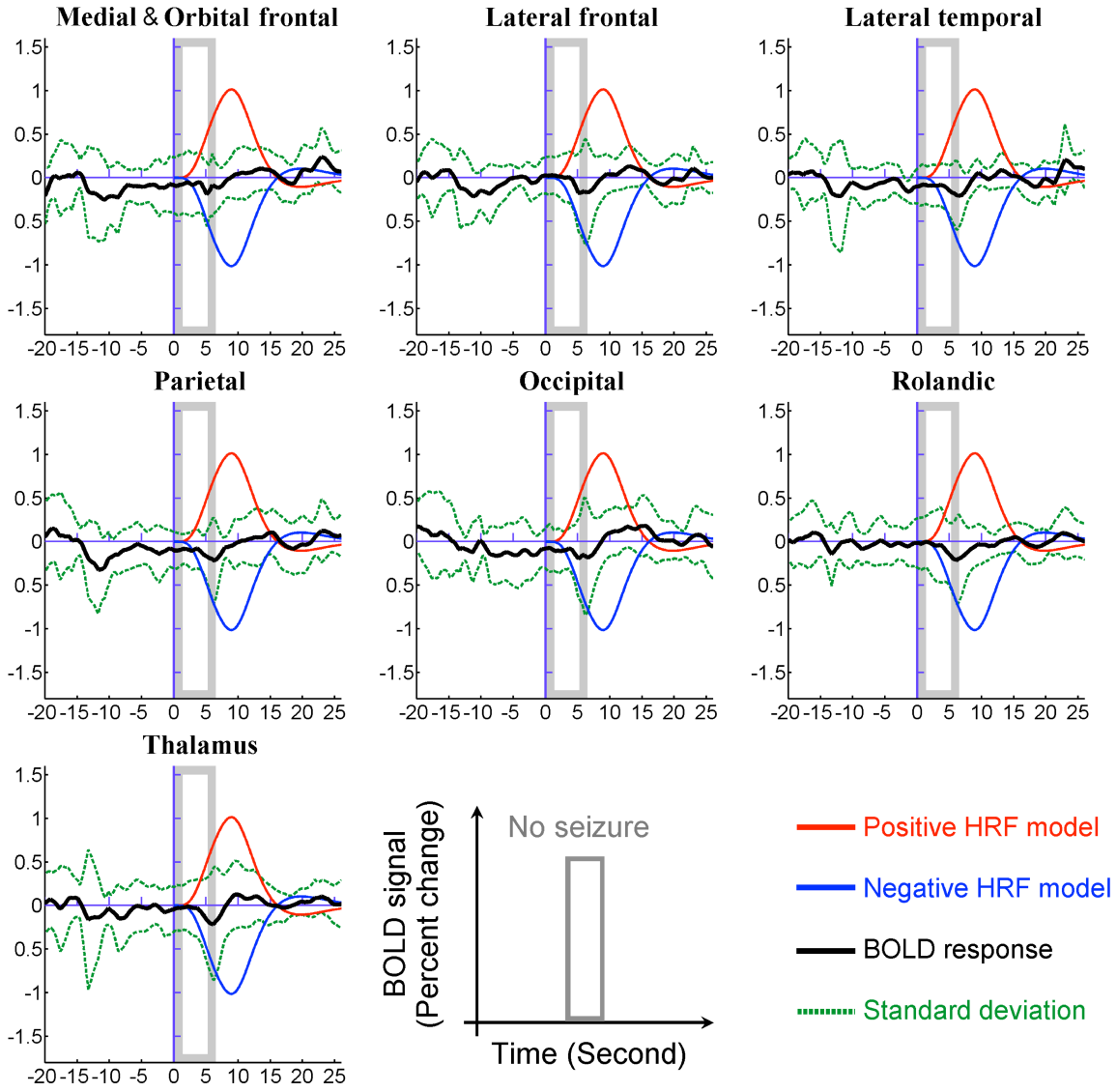

Figure 17. fMRI timecourses during no seizure periods. Mean fMRI timecourses in 7 anatomical VOIs (see Fig. 6 for VOIs/regions). We performed a group analysis using the same number of data segments, with identical timing with respect to behavioral tasks, and from the same patients as Fig 16, but during times when no seizures occurred. Red and blue curves represent the positive and negative HRF models obtained by convolving a boxcar function of 6.6s (mean seizure duration, shown in gray) with the canonical HRF of SPM2. Data for no seizure periods are the same as in Fig 15. (Reprinted with permission from Bai, X *et al,* 2010).

Chapter 4: Discussion, Conclusions, and Future Directions

4A: Ictal Imaging: Discussion and Conclusions

The aim of this part of this thesis was to use simultaneous EEG, fMRI and behavioral testing to investigate the neural networks involved in absence seizures that impair behavior. To our knowledge, this is the first study to combine ictal EEG-fMRI recording with simultaneous behavioral testing.

In this study we demonstrated that there were fMRI signal changes that were associated with behavioral impairment, particularly on a task of attentional vigilance. In agreement with previous studies of simultaneous EEG-fMRI in CAE populations, we demonstrated that, in seizures with ictal behavioral impairment, there were increases in fMRI BOLD signal in the thalamus, frontal cortex, primary somatosensory cortex, primary motor cortex, primary visual cortex, and primary auditory cortex as well as decreases in the lateral parietal, medial parietal, and anterior cingulated cortices, basal ganglia, pons and cerebellum (18 – 28).

It is our hypothesis that the ictal fMRI changes are manifestations of involvement of two neuronal networks that are key to the type of attentional/arousal deficits present during absence seizures. The first of these neural networks is the thalamus and frontal cortex that are the primary drivers of attention via increasing arousal and association of sensory inputs. The second of the neural networks we hypothesize is involved in the fMRI changes associated with behavioral impairment during absence seizures are the sensory and attentional integrators of the primary sensory and motor cortices. It is our hypothesis that there must be disruption of both of these systems in order to bring about the attentional impairments seen in absence seizures.

This study also was consistent with ictal fMRI signal decreases seen in previous studies (18 – 28). We showed ictal decreases in what are traditionally referred to as default mode areas: lateral and medial parietal cortices along with cingulate cortex and basal ganglia. Default mode areas are referred to as such as they are constitutively active during awake, conscious states. It is quite possible that deactivation of these areas that are constitutively "on" during awake behaving conscious states could contribute to loss of consciousness observed during absence seizures.

This study was unique in its use of behavioral testing during simultaneous EEG-fMRI, though its conclusions agree with previous behavioral examinations of CAE patients in that this study also demonstrated that, ictally, children have more difficulty with tasks requiring attention than with tasks requiring simple repetitive behavior (i.e. more difficulty with CPT as compared to RTT) (14). When this observation is paired with the fMRI findings of this study one possible explanation for this attentional impairment becomes more apparent in that traditional attention and arousal areas (thalamus, and frontal association cortex) are those showing the largest changes in ictal fMRI signal.

Children with CAE, have attentional deficits interictally as well as ictally, and it would be interesting to examine possible interictal fMRI changes in attention-associated neural networks in these subjects (6, 8). It is possible that CAE subjects have differences in interictal fMRI activity while performing an attentional task when compared to control children, and it would be potentially interesting to examine the locations of these potential interictal fMRI signal differences.

The current study also, interestingly, lends more evidence to the notion that absence seizures might not necessarily be a globally distributed form of generalized epilepsy as described in the above introduction (3, 6). The above data (i.e. the fMRI changes in focal brain areas, as opposed to the whole brain, during seizures) lends credence to the possibility that absence epilepsy could be simply a combination of focal disorders in neural networks that ends up having a global effect on consciousness.

This study also agrees with past behavioral CAE experiments that showed children with CAE to have variable behavioral impairments between similar seizure episodes (i.e. similar SWD patterns in the same subject will produce different behavioral degrees or types of behavioral impairment) (6, 14). Though this study was not sufficiently powered to address such a question, it is possible that differential involvement of particular neural networks is predictive of the type of behavioral impairment present during a single seizure.

There were many limitations to the current study, not the least of which was the small sample size and the resultant few numbers of seizures with concomitant behavioral testing. Additionally, the CPT utilized, by stressing general attentional vigilance, is not directed at testing one particular form of attention over another. Similarly, the RTT utilized required some degree of attentional vigilance so that subjects could continually watch the letter presentation and maintain the 1 Hz button-press/letter-presentation cadence (14). In the end, subjects were also able to utilize many different attentional or motoric mental strategies to perform both the CPT and RTT and these differential strategies across subjects could have influenced the ictal performance or fMRI activity reported above. Additionally, such a study is always made exponentially more difficult as

the study necessitates seizures during behavioral tasks while at the same time decreasing seizure frequency by forcing subjects to engage in tasks that require attentional vigilance and therefore decrease seizure frequency (6).

Many exciting avenues exist for the further pursuit of this work, including the possible correlation of particular ictal fMRI patterns of change with specific behavioral impairments on behavioral tasks (56). It is possible that subjects with more thalamic activation would perform more poorly on an attentional task or even that some ictal neural network activity could be protective of ictal behavioral performance. These possibilities leave open various non-pharmacological avenues for therapy, including possible ictal attentional strategies to counteract the disruption of various neural networks during seizures. Additionally, and in direct relevance to the second aim of this thesis, it would be interesting to examine whether the ictal timecourse of fMRI changes has any influence on behavioral performance.

4B: Ictal Timecourse: Discussion and Conclusions

The purpose of this arm of the thesis was to investigate the timecourse of ictal fMRI signal change. In doing so, we developed a novel, data-driven method for looking at changes in fMRI BOLD signal over time. This method used a voxel-based examination of volumes of interest to examine the simple percentage change in fMRI signal over time, both ictally as well as pre- and post-ictally. When compared to the general linear model normally used in fMRI analysis (i.e. a double gamma function of the traditional HRF convolved with the boxcar function of seizure onset and offset (50)), our model better allows for the examination of signal change over time.

When examining the frequency timecourse of the EEG data, we found that the SWDs included in the study had characteristic frequencies of 3 – 4 Hz. Interestingly, however, seizures seemed to start at a characteristic frequency closer to 4 Hz and then slow to 3 Hz throughout the duration of the seizure. This slowing of SWD fits well with the pathophysiology of SWD generation and could perhaps be explained by the recruitment of more $GABA_B$ receptors and concomitant increase in thalamic IPSP as the seizure lasts longer.

Behaviorally, as has been shown in previous studies, we demonstrated that participants performed more poorly on tasks involving ictal attentional vigilance than on tasks that required simple motor performance (i.e. worse performance on CPT than on RTT) (6, 14). We also found that behavioral impairment is tightly temporally correlated with ictal activity. Behavioral impairments, whether on CPT or RTT, start and end abruptly with SWD onset and offset (14, 57 - 60).

Additionally, we hypothesized that fMRI signal change important to the understanding of SWD and absence seizures occurs not only during the electrographic period of SWD presence. Using the voxel-based percent change maps, we were able to examine not only the ictal fMRI changes, but also the fMRI activity and its change over time both pre- and post-ictally. Using this method we found that, indeed, the GLM of absence seizures did not truly reflect the fMRI signal changes over time.

We found a sequence of signal changes that evolved over time: early fMRI signal increases were seen well before seizure onset in medial orbital frontal, frontal polar, cingulate, lateral parietal, precuneus, and lateral occipital cortex; after seizure onset, fMRI increases progressed to also involve lateral frontal and temporal cortex; following

the end of seizures, fMRI increases were seen in the medial occipital cortex, and lastly in the thalamus. fMRI signal decreases occurred later, and continued well after seizure end. Decreases were observed initially in medial/orbital frontal, cingulate, medial and lateral parietal cortices, followed by decreases in lateral frontal, temporal and occipital cortices, and basal ganglia. In examination of these changes, it is interesting to note that they begin up to 14 seconds before and up to 24 seconds after the onset of SWD. Taking the fMRI changes as a whole, they seem to be easily divided into three categories, early increases from -8 sec - +4 seconds, followed by increases and decreases from +8 sec - 14 sec and then by only decreases after + 16 sec relative to seizure onset. Though this is the first study of its kind to look at changes in fMRI activity over time, the period of late decreases seen after 16 seconds is consistent with another recent study that looked at late seizure changes by shifting the HRF examination after seizure offset (18, 55).

Based upon the above observations, it is our assertion that the characteristics of absence seizures, including associated ictal behavioral impairment, are influenced not only by the particular neural networks affected, but also by the sequence in which those neural networks are affected. The whole story of absence seizures is not likely contained in the short time window between the onset and offset of SWDs. Based on the above data, it is equally important to examine neural and fMRI changes occurring within the pre- and post-ictal periods as well.

Most notably, this study demonstrates the importance of the examination of fMRI results in a data-driven manner rather than simply feeding everything into a system bound by the constraints of the GLM and traditional HRF. As was demonstrated in the comparison between the voxel-based and GLM models, there is clearly more ictal

activity associated with absence epilepsy than is expressed using the GLM. In fact, the GLM will even, at times, mask the demonstration of several neural networks with clear fMRI changes in our model (e.g. lateral frontal and lateral temporal activations discussed above). Examining the data by blindly using only the GLM is in many ways like trying to examine a square peg after it has been forced though a round hole. In processing the fMRI signal and then fitting it into the constraints of a model like the GLM, one loses much knowledge about the original data in the process.

As is demonstrated in the case of the thalamus, the closer the data fits the model, the stronger the displayed results will be after GLM analysis. This is clearly not the full story of the fMRI activity that underlies absence seizures, however, as this method simply overlooks data that does not fit neatly within the model -- even at times, misinterpreting that data. For example, as cited above, it is possible that the decreases seen in "default mode' areas in previous studies are simply a manifestation of the GLM's misinterpretation of early activations in those areas (20, 24).

Additionally, the above results lend evidence to the rejection of the view of absence seizures as a form of generalized global epilepsy (6). From our data, it is clear that there are focal areas of fMRI change occurring in separate neural networks throughout the timecourse of the seizure, not simply pan-cortical activity.

Interestingly, though, when the fMRI timecourse is compared to the timecourse of the behavioral changes associated with absence seizures, there is a stark contrast between fMRI changes that begin before and outlast SWD and behavioral changes that are more tightly temporally correlated with the period of SWDs. There could be many reasons for this including the possibility that the fMRI changes that we observe do not truly reflect

the underlying ictal neural activity. It is also possible that, although many areas are involved in the fMRI changes that surround absence seizures, there is one particular area whose involvement is both necessary and sufficient to cause behavioral impairment. Additionally, a particular activation sequence of ordered neural network activation might be necessary to trigger the characteristic behavioral deficits associated with absence seizures in CAE. In these cases, it would be the involvement of this neural network or specific temporal pattern of activation of neural networks that would be most associated in time with both SWD on EEG and the abrupt onset of behavioral changes that are the characteristic phenotype of absence epilepsy.

In conclusion, the above findings reveal a complex and long-lasting sequence of fMRI changes in CAE absence seizures that are not detectable by conventional HRF modeling. These findings, together with general knowledge of the timecourse of fMRI signal change during absence seizures, will likely reveal important underpinnings of absence epilepsy and are ultimately important in the understanding and eventual treatment of childhood absence epilepsy.

4C: Future Directions

This research has spawned many different exciting avenues that could easily be taken up in the future. With many more questions arising than answers from this particular set of studies, the natural follow up to this thesis would be an investigation that tries to better associate changes in fMRI signal with particular deficits in behavior. For example, it would be incredibly interesting to examine whether activation of a particular neural network or activation of neural networks in a certain timecourse would predict

impairment on a given task of attention. If one were to attempt such a study using only ictal impaired behavior, though, it would prove to be exceedingly difficult as the number of seizures with behavioral testing that one would need to sufficiently power such an experiment would be orders of magnitude higher than the number of seizures used to generate the results found in this thesis.

One area, however, that lends itself to this type of investigation, is the interictal deficits in attentional vigilance present in the CAE population. Though these interictal attentional deficits are much subtle than those ictal deficits explored above, there is the potential for much more interictal behavioral testing and therefore, much more power behind the potential correlation of interictal fMRI changes with particular behavioral impairments.

Additionally, much research has been done in an effort to not simply treat CAE, but instead to cure it. Of note, a recent study looking at the epileptogenesis of CAE in a Wag/Rij model of absence epilepsy, demonstrated the ability to prevent development of seizures, if animals that were genetically predestined to develop the disease were treated with ethosuximide before seizures began (61). As such, there is much work to be done in order to elucidate the course of epileptogenesis in the CAE population -- including the investigation of possible non-invasive biomarkers of disease development that could then be used to identify patients who might benefit from the potential for such early curative intervention.

In this regard, future work looking at such markers would be quite interesting and possibly helpful in the treatment of CAE. Ongoing studies looking at non-invasive hematological, functional, and anatomical indicators of the development of CAE are

currently underway (32, 56). With the results and techniques brought to light by the current body of work, there is tremendous potential to make significant headway towards the understanding, treatment, and possible cure for childhood absence epilepsy.

References

1. Radhakrishnan, K. June, 2009. Challenges in the management of epilepsy in resource-poor countries. *Nature Reviews Neurology*. 5: 323-330.

2. Berg, A.T., Berkovic, S.F., Brodie, M.J., Buchhalter, J., Cross, J.H. *et al*. 2010. Revised terminology and concepts for organization of seizures and epilepsies: Report of the ILAE Commission on Classification and Terminology, 2005 - 2009. *Epilepsia*. 51 (4). 676 – 685.

3. Commission on classification and terminology of the international league against epilepsy: Proposal for revised classification of epilepsies and epileptic syndromes (1989). *Epilepsia.* 30: 389-399.

4. Commission on classification and terminology of the international league against epilepsy: Proposal for revised clinical and electrographic classification of epileptic seizures (1981). *Epilepsia.* 22: 489-501.

5. Vestal, M.L., and Blumenfeld, H. 2010. Pathophysiology of absence seizures. In *Atlas of Epilepsies*. CP Panayiotopoylos, editor. New York: Springer. In press.

6. Blumenfeld, H. 2005. Consciousness and epilepsy: why are patients with absence seizures absent? Prog Brain Res 150: 271 - 286

7. Shorvon, S. 2005 *Handbook of epilepsy treatment: forms, causes and therapy in chldren and adults*. 2nd Ed. Oxford: Blackwell publishing. 304 pp.

8. Camfield, P. and Camfield C. 2002. Epileptic syndromes in childhood: clinical features, outcomes, and treatment. *Epilepsia*. 43 (Suppl 3). 27-32.

9. Wirrell, E. 2003. Natural history of absence epilepsy in children. *Can. J. Neurol. Sci.* 30: 184 – 188.

10. Wirrell, E., Camfield C., Camfield P., Dooley, J., Gordon, K., *et al*. 1997. Long-term psychosocial outcome in typical absence epilepsy: sometimes a wolf in sheep's clothing. *Arch Pediatr Adolesc Med.*151: 152–8.

11. Blumenfeld, H., and Coulter, D. 2008. Thalamocortical anatomy and physiology. In: *Epilepsy: A Comprehensive Textbook, 2nd Edition*. J. Engel, Jr. and T. A. Pedley, editors. Philadelphia: Lippincott Williams & Wilkins. Ch 31: 353-366.

12. Blumefeld, H., and McCormick, D. 2000. Corticothalamic inputs control the pattern of activity generated in thalamocortical networks. *J Neurosci.* 20 (13): 5153 – 5162.

13. Davidoff, R., and Johnson, L. 1964. Paroxysmal EEG activity and cognitive-motor performance. *Electroenceph and Clin Neurophysiol*. 16: 343-354.

14. Mirsky, A.F., and Buren J.M.V. 1965. On the nature of the "absence" in centrencephalic epilepsy: a study of some behavioral, electroencephalographic and autonomic factors. *Electroencephalogr Clin Neurophysiol*. 18: 334-348.

15. Sadleir, L.G., Farrell, K., Smith, S., Connolly, M.B., and Scheffer, I.E. 2006. Electroclinical features of absence seizures in childhood absence epilepsy. *Neurology*. 67: 413-8.

16. Sadleir, L.G., Scheffer, I.E., Smith, S., Carstensen, B., Farrell, K., Connolly, M.B. 2009. EEG features of absence seizures in idiopathic generalized epilepsy: impact of syndrome, age, and state. *Epilepsia*. 50: 1572-8.

17. Shimazono, Y., Hirai, T., Okuma, T., Fukuda, T., Yamamasu, E. 1953 Disturbance of consciousness in petit mal epilepsy. *Epilepsia*. 2:49-55.

18. Aghakhani, Y., Bagshaw, A.P., Benar, C.G., Hawco, C., Andermann, F., Dubeau, F., *et al*. 2004. fMRI activation during spike and wave discharges in idiopathic generalized epilepsy. *Brain*. 127: 1127-1144.

19. Archer, J.S., Abbott, D.F., Waites, A.B., and Jackson, G.D. 2003. fMRI "deactivation" of the posterior cingulated during generalized spike and wave. *Neuroimage*. 20: 1915-1922.

20. Gotman, J., Grova, C., Bagshaw, A., Kobayshi, E., Aghakhani, Y., and Dubeau, F. 2005. Generalized epileptic discharges show thalamocortical activation and suspension of the default state of the brain. *Proc. Natl. Acad. Sci. USA*. 102: 15236-15240.

21. Hamandi, K., Salek-Haddadi, A., Laufs, H., Liston, A., Friston, K., Fish, D.R., *et al*. 2006. EEG-fMRI of idiopathic and secondarily generalized epilepsies. *Neuroimage*. 31: 1700-1710.

22. Hawco, C.S., Bagshaw, A.P., Lu, Y., Dubeau, F., and Gotman, J. 2007. BOLD changes occur prior to epileptic spikes seen on scalp EEG. *Neuroimage*. 35: 1450-8.

23. Labate, A., Briellmann, R., Abbott, D., Waites, A., and Jackson, G. 2005. Typical childhood absence seizures are associated with thalamic activation. *Epileptic Disorders*. 7: 373-377.

24. Laufs, H., Lengler, U., Hamandi, K., Kleinschmidt, A., and Krakow, K. 2006. Linking generalized spike-and-wave discharges and resting state brain activity by using EEG/fMRI in a patient with absence seizures. *Epilepsia*. 47: 444-448.

25. Moeller, F., Siebner, H.R., Wolff, S., Muhle, H., Boor, R., Granert, O., *et al*. 2008. Changes in activity of striato-thalamo-cortical network precede generalized spike wave discharges. *Neuroimage.* 39: 1839-1849.

26. Moeller, F., Siebner, H.R., Wolff, S., Muhle, H., Granert, O., Jansen, J.F., *et al*. 2008. Simultaneous EEG-Fmri in drug-naive children with newly diagnosed absence epilepsy. *Epilepsia*. 49:1510-1519.

27. Salek-Haddadi, A., Lemieux, L., Merschhemke, M., Friston, K., Duncan, J., and Fish, D. 2003. Functional magnetic resonance imaging of human absence seizures. *Ann Neurol*. 53: 663-667.

28. Vaudano, A.E., Laufs, H., Kiebel, S.J., Carmichael, D.W., Hamandi, K., Guye M, *et al*. 2009. Causal hierarchy within the thalamo-cortical network in spike and wave discharges. *PLoS One*. 4(8): e6475: 1-11.

29. Carmichael, D.W., Hamandi, K., Laufs, H., Duncan, J.S., Thomas, D.L., and Lemieux, L. 2008. An investigation of the relationship between BOLD and perfusion signal changes during epileptic generalised spike wave activity. *Magn Reson Imaging*. 7: 870 - 3.

30. Nersesyan, H., Hyder, F., Rothman, D., and Blumenfeld, H. 2004. Dynamic fMRI and EEG recordings during spike-wave seizures and generalized tonic-clonic seizures in WAG/Rij rats. *J Cereb Blood Flow Metab*. 24:589-599.

31. Nersesyan, H., Herman, P., Erdogan, E., Hyder, F., Blumenfeld H. 2004. Relative changes in cerebral blood flow and neuronal activity in local microdomains during generalized seizures. *J Cereb Blood Flow Metab*. 24:1057-1068

32. Mishra, A.M., Ellens, D.J., Schridde, U., Motelow, J.M., Purcaro, M., Hyder, F., Blumenfeld, H. 2008. Simultaneous fMRI/CBV and EEG during spike-wave seizures in WAG/Rij rat. *Proc Intl Soc Mag Reson Med Toronto, Canada*. 582. (Abstr.)

33. Barceloux, M. 1998. *Medical Toxicology of Natural Substances*. New York: Elsevier. 1157 pp.

34. Buchanan, R., and Kinkel A. 1969. Absorption and elimination of ethosuximide in children. *J Clin Pharmacol*. 25: 513.

35. Chen, C., Casale, E.J., Duncan, B., Culverhouse, E.H., and Gilman, J. 1999. Pharmacokinetics of Lamotrigine in Children in the Absence of other Antiepileptic Drugs. *Pharmacotherapy*. 19: 437-451.

36. Hvidberg, E.D. Clinical pharmacokinetics of anticonvulsants. 1976. *Clin Pharmacokinet*. 1: 161-178.

37. Negishi, M., Abildgaard, M., Laufer, I., Nixon, T., and Constable, R. 2008. An

EEG (electroencephalogram) recording system with carbon wire electrodes for simultaneous EEG-fMRI (functional magnetic resonance imaging) recording. *J Neurosci Methods*. 173: 99-107.

38. Negishi, M., Abildgaard, M., Nixon, T., and Constable, R. 2004. Removal of time-varying gradient artifacts from EEG data acquired during continuous fMRI. *Clinical Neurophysiology*. 115: 2181-2192.

39. Genovese, C.R., Lazar, N.A., and Nichols, T. 2002. Thresholding of statistical maps in functional neuroimaging using the false discovery rate. *Neuroimage*. 15:870-878.

40. Langers, D.R., Jansen, J.F., and Backes, W.H. 2007. Enhanced signal detection in neuroimaging by means of regional control of the global false discovery rate. *Neuroimage*. 38: 43-56.

41. Schwartzman, A., Dougherty, R.F., Lee, J., Ghahremani, D., and Taylor, J.E. 2009. Empirical null and false discovery rate analysis in neuroimaging. *Neuroimage*. 44 (1): 71 - 82.

42. Jus, A., and Jus, C. 1960. Etude electro-clinique des alterations de conscience dans le petit mal. *Studii si cercetari de Neurol*. 5: 243-254.

43. Yeager, C.L., and Guerrant, J.S. 1957. Subclinical epileptic seizures; impairment of motor performance and derivative difficulties. *Calif Med*. 86: 242-247.

44. Miezin, F., Maccotta, L., Ollinger, J., Petersen, S., and Buckner, R. 2000. Characterizing the hemodynamic response: effects of presentation rate, sampling procedure, and the possibility of ordering brain activity based on relative timing. *Neuroimage*. 11: 735-759.

45. Neumann, J., Lohmann, G., Zysset, S., and von Cramon, D. 2003. Within-subject variability of BOLD response dynamics. *Neuroimage*. 19: 784-796.

46. Handwerker, D., Ollinger, J., and D'Esposito, M. 2004. Variation of BOLD hemodynamic responses across subjects and brain regions and their effects on statistical analyses. *Neuroimage*. 21: 1639-1651.

47. Meltzer, J.A., Negishi, M., and Constable, R. 2008. Biphasic hemodynamic responses influence deactivation and may mask activation in block-design fMRI paradigms. *Hum Brain Map*. 29: 385-399.

48. Amor, F., Baillet, S., Navarro, V., Adam, C., Martinerie, J., and Le Van Quyen, M. 2009. Cortical local and long range synchronization interplay in human absence seizure initiation. *Neuroimage*. 45: 950-962.

49. Oppenheim, A.V., and Schafer, R.W. 1989. *Discrete-Time Signal Processing*. Englewood Cliffs, NJ: Prentice-Hall. 870 pp.

50. Friston, K.J., Holmes, A.P., Worsley, K.P., Poline, J.B., Frith, C., and Frackowiak, R.S.J. 1995. Statistical parametric maps in functional imaging: a general linear approach. *Hum Brain Map*. 2: 189-210.

51. Glover, G.H. 1999. Deconvolution of impulse response in event-realted BOLD fMRI. *Neuroimage*. 9: 416-466.

52. Tzourio-Mazoyer, N., Landeau, B., Papathanassiou, D., Crivello, F., Etard, O., Delcroix, N., *et al*. 2002. Automated anatomical labeling of activations in SPM using a macroscopic anatomical parcellation of the MNI MRI single-subject brain. *Neuroimage*. 15: 273-289.

53. Bai, X., Vestal, M., Berman, R., Negishi, M., Spann, M., Vega, C., DeSalvo, M., Novotny, E.J., Constable, R.T., and Blumenfeld, H. 2010. Dynamic timecourse of typical childhood absence seizures: EEG, behavior and fMRI. *Journal of Neuroscience,* In press.

54. Vaudano, A.E., Laufs, H., Kiebel, S.J., Carmichael, D.W., Hamandi, K., Guye, M., *et al*. 2009. Causal hierarchy within the thalamo-cortical network in spike and wave discharges. *PLoS One*. 4(8): e6475: 1-11.

55. Gotman, J., Kobayashi, E., Bagshaw, A.P., Benar, C.G., and Dubeau, F. 2006. Combining EEG and fMRI: a multimodal tool for epilepsy research. *Journal of Magnetic Resonance Imaging*. 23: 906-20.

56. Vestal, M.L., Bai, X., Negishi, M., Berman, R., Vega, C., Spann, M., DeSalvo, M., McAuliffe, C.L., Novotny, E.J., Constable, R.T., and Blumenfeld, H. 2009. Childhood absence epilepsy: functional neuroimaging of interical attention. *Epilepsia*. Suppl 0. (Abstr.)

57. Bates, J.A.V. 1953. A technique for identifying changes in consciousness. *Electroenceph and Clin Neurophysiol*. 5: 445-446.

58. Goode, D.J., Penry, J.K., and Dreifuss, F.E. 1970. Effects of Paroxysmal Spike-Wave on Continuous Visual-Motor Performance. *Epilepsia*. 11: 241-254.

59. Tizard, B., and Margerison, J.H. 1963. The relationship between generalized and paroxysmal EEG discharges and various test situations in two epileptic patients. *J Neurol Neurosurg Psychiatry*. 26.

60. Panayiotopoulos, C.P., Obeid, T., and Waheed, G. 1989. Differentiation of typical absence seizures in epileptic syndromes: a video-EEG study of 124 seizures in 20 patients. *Brain*. 112: 1039-1056.

61. Blumenfeld, H., Klein, J.P., Schridde, U., Vestal, M.L., Rice, T., *et al*. 2008. Early treatment suppresses the development of spike-wave epilepsy in a rat model. *Epilepsia*. 49(3): 400-409.